

Coupled-channel study of axial-vector mesons with realistic t- and u-channel exchanges

Vom Fachbereich Physik
der Technischen Universität Darmstadt

zur Erlangung des Grades
eines Doktors der Naturwissenschaften
(Dr. rer. nat.)

genehmigte Dissertation von
Dipl.-Phys. Julian Hofmann
aus Frankfurt a.M.

Referent: Priv. Doz. Dr. Matthias F.M. Lutz

Korreferent: Prof. Dr. Christian Fischer

Tag der Einreichung: 25.1.2010

Tag der Prüfung: 17.2.2010

Darmstadt 2010

D17

Contents

1	Zusammenfassung	5
2	Introduction	7
3	The tree-level scattering amplitude	9
3.1	Introduction: QCD and Effective Theories	9
3.1.1	Color	9
3.1.2	Flavor	10
3.2	The interaction	11
3.3	Partial wave projection	14
4	Analytic structure of the potential	23
4.1	The potential from dispersion integrals	26
4.1.1	Example: the exchange of a kaon in $\pi \rho \rightarrow K \bar{K}^*$	29
4.2	Perturbative analysis of the scattering amplitude	32
4.2.1	Anomalous thresholds	34
4.2.2	Cuts on the real axis: $\pi \rho \rightarrow \pi \rho$	36
4.2.3	Cuts on the real axis: $\pi \phi \rightarrow \bar{K} K^*$	38
4.2.4	Cuts on the real axis: $\pi K^* \rightarrow K \rho$	38
5	Computation of the scattering amplitude	41
5.1	Case 1: real potential	41
5.2	Case 2: complex potential	42
6	Results	47
6.1	Results for Weinberg-Tomozawa Interaction	47
6.1.1	$(I, S) = (\frac{1}{2}, 1)$	47
6.1.2	$(I^G, S) = (0^+, 0)$	49
6.1.3	$(I^G, S) = (0^-, 0)$	51
6.1.4	$(I^G, S) = (1^+, 0)$	51
6.1.5	$(I^G, S) = (1^-, 0)$	53
6.2	Results for the full interaction	54
6.2.1	$(I^G, S) = (1^+, 0)$: the $b_1(1235)$	54
6.2.2	$(I, S) = (\frac{1}{2}, 1)$: the $K_1(1270)$	58

7	Summary and Outlook	61
A	The invariant amplitude	63
A.1	The 4-point vertices	63
A.2	The Pseudoscalar s-channel Exchange	64
A.3	The Pseudoscalar u-channel Exchange	64
A.4	The s-channel Vector Exchange	64
A.5	The t-channel Vector Exchange	66
A.6	The u-channel Vector Exchange	66

Chapter 1

Zusammenfassung

Aufgabe der theoretischen Hadronenspektroskopie ist es, Eigenschaften von mesonischen und baryonischen Resonanzen, wie zum Beispiel Massen und Partialbreiten, zu berechnen. Ein möglicher Weg hierzu ist das Quark-Modell, in dem Grundzustand und Anregungszustände von Systemen aus Quarks und Antiquarks (und Gluonen) berechnet werden.

Ziel dieser Arbeit ist es, einen Teil des mesonischen Spektrums genauer zu untersuchen. Der hier verwendete Ansatz ist nicht das Quarkmodell. Als Freiheitsgrade werden nicht Quarks und Gluonen verwendet, sondern die Mesonen selbst. Ziel ist es, die Amplitude für die Streuung der leichtesten pseudoskalaren Mesonen, der SU(3) Goldstone Bosonen (π , K , η), an den Vektormesonen ρ , K^* und ω nicht-perturbativ zu berechnen. Resonanzen manifestieren sich als Pole in der Streuamplitude.

Ein Formalismus, der schon mehrfach eingesetzt wurde, um die Streuamplitude nicht-perturbativ zu berechnen ist das Lösen einer partialwellen-projezierten Bethe-Salpeter-Gleichung. Hierzu wird die Streuamplitude zuerst in Störungstheorie berechnet, anschliessend partialwellen-projeziert und als Kern für eine Bethe-Salpeter-Gleichung verwendet. Als Modell für die Wechselwirkung wurde typischerweise der chirale Lagrangian in führender Ordnung verwendet. Meist wurde nur s-Wellen Streuung betrachtet. Die Behandlung der Energieabhängigkeit einer Wechselwirkung, die s -, t - und u -Kanal Austauschprozesse beinhaltet, ist schwierig.

In dieser Arbeit wird ein Formalismus verwendet, der nicht die Bethe-Salpeter-Gleichung benutzt, sondern auf einer nicht-linearen Integralgleichung basiert. Lösungen dieser Gleichung sind kausal und analytisch. Der Input in diese Gleichung ist ein vorbehandeltes Potential. Um dieses zu erhalten sind mehrere Schritte nötig. Eine Lagrange-Dichte, die mit einer Kombination aus chiralen und Large- N_c Argumenten aufgestellt wurde, wird aus einer früheren Arbeit übernommen und verwendet, um die Streuamplitude in Störungstheorie zu berechnen. Enthalten sind neben der führenden chiralen Ordnung sowohl Gegenterme als auch pseudoskalare und vektorielle Austauschprozesse. Das Ergebnis wird partialwellen-projeziert und – unter Ausnutzung seiner analytischen Eigenschaften – zu höheren Energien extrapoliert. In

dieser Form kann das Potential nun verwendet werden, um die volle Streuamplitude zu berechnen.

In einem ersten Schritt geschieht das für ein Potential, in dem nur die Weinberg-Tomozawa-Wechselwirkung berücksichtigt wird. Dies erlaubt einen Vergleich mit früheren Ergebnissen, bei denen das gleiche System mit Hilfe der Bethe-Salpeter-Gleichung untersucht wurde. Im nächsten Schritt wird die vollständige Wechselwirkung verwendet, um das $b_1(1235)$ und das $K_1(1270)$ genauer zu betrachten. Das Potential enthält noch zwei unbekannte Kopplungskonstanten, die an das experimentelle Spektrum angepasst werden können. Die hierbei erhaltenen Werte sind zwar konsistent mit früheren Rechnungen, jedoch unterscheiden sie sich signifikant für die beiden Resonanzen. Dies wird als eine Konsequenz der Abwesenheit von pseudoskalaren Austauschprozessen interpretiert.

Wegen technischer Probleme wurden diese in der finalen Rechnung weggelassen. Das ist auch der Grund, warum weitere relevante Grössen, wie zum Beispiel das D/S Verhältnis der Zerfälle der betrachteten Resonanzen, nicht genauer untersucht wurden. Die Ursachen des technischen Problems werden erläutert und ein möglicher Lösungsweg diskutiert. Interessant für weitere Arbeiten ist zum einen der Einfluss dieser Prozesse auf das Spektrum. Zum anderen können mit den in dieser Arbeit verwendeten Methoden auch Vektor-Vektor- und Pseudoskalar-Pseudoskalar Kanäle in das Modell mit einbezogen werden. Dadurch würde die Behandlung von Resonanzen mit höheren Spins interessant.

Chapter 2

Introduction

The accepted theory of the strong interaction is QCD. It describes the coupling of the six known quarks, three of which are light, and the gluons. This interaction is based on the gauge group $SU(3)$ that couples to an internal quantum number called color. Since this gauge group is non-Abelian, the gluons can interact with themselves. Another remarkable feature of QCD is that the renormalized coupling constant is large at low energies. This invalidates standard perturbation theory. A perturbative expansion is meaningful only at high energies.

Although the details are not completely understood yet, this leads to an interesting effect at low energies: confinement. Color-neutral particles are the only hadrons observed in nature. These are divided into the bosonic mesons and fermionic baryons. The calculation of the properties of these composite particles, mass and partial decay widths, is the task of theoretical hadron spectroscopy. A traditional way to do so is to model for example a meson as a bound quark-antiquark state [1, 2, 3].

The approach followed in this thesis is based on a different idea: at low energies an expansion of quark interactions in powers of the QCD coupling constant is impossible. The relevant degrees of freedom at these energies are the baryons and mesons and not quarks and gluons. Hadronic resonances manifest themselves as poles in scattering amplitudes. The ansatz used here is to calculate these scattering amplitudes with baryons and mesons as the relevant degrees of freedom.

Because of spontaneous chiral symmetry breaking the interaction of the lightest hadrons – the flavor $SU(3)$ multiplet containing the pion, also called pseudo-Goldstone Bosons – with any other hadron can be expanded in powers of small momenta and the small quark masses. At leading order, this interaction depends exclusively on a single parameter, the pion decay constant f_π . To calculate non-perturbative effects like bound states or resonances from this leading order interaction, an infinite summation is needed. In previous works this was provided by the Bethe-Salpeter-Equation (BSE). S-wave bound states of the Goldstone Bosons with a variety of other hadrons have been calculated within this formalism. In [4, 5, 6] the scattering ampli-

tude of the Goldstone Bosons with the SU(3)-multiplet including the nucleon has been calculated. In [7, 8] the Goldstone Bosons were scattered off the charmed sextet containing the Σ_c and the anti-triplet containing the Λ_c . The works [9, 10, 11] considered the interaction of the baryon resonances with spin and parity $3/2^+$, the multiplets containing the Δ and the Σ_c^* . The interaction of the Goldstone bosons with the lightest vector mesons (ρ , K^* , ϕ and ω) were subject of [15, 16]. Charmed mesons were studied in [12, 13, 14] and together with hidden charm in [17].

In summary one can say that the framework used works extremely well whenever the Goldstone Bosons are interacting with spin 0 or spin 1/2 particles. In the case of spin 1 or 3/2 particles the agreement is more schematic. The problem is that for example in $\pi \Delta$ scattering the ρN channel is ignored even so it is not much heavier. A more realistic model needs to consider take additional channels, together with a more elaborate interaction that includes s , t and u -channel exchange processes. Such additional terms in the interaction will lead to a more complicated analytic structure of the interaction kernel. A different scheme is necessary to unitarize the tree-level scattering amplitudes. This scheme is provided in [18]. In that work the scattering of the nucleon octet off the light pseudoscalar and vector mesons is studied. Non-linear integral equations that are based on causal and unitarity properties of the scattering amplitude are employed to unitarize the scattering kernel.

In this thesis this scheme will be used to examine resonances in the scattering of the light pseudoscalar (P) and vector (V) mesons. This allows for a more realistic interaction than in [15]. Also the d-wave amplitude will be calculated, making additional observables like the D/S ratio for the $b_1(1235)$ accessible. The inclusion of additional channels (PP or VV) is beyond the scope of this work, but a desirable next step.

This work is organized as follows: in the subsequent section the tree-level amplitude for the interaction of a light pseudoscalar meson with a vector meson (PV \rightarrow PV) will be calculated and partial-wave projected. The interaction Lagrangian is taken from [19] where it was constructed using chiral and large N_c arguments.

In the third chapter the resulting potential will be modified such that it can be used as an input for the non-linear integral equations on which this approach is based. Several technical problems can occur in that process and will be discussed in detail. The methods to solve the dispersion relations for the full scattering amplitude are summarized in the following chapter. Finally the results will be presented. A short summary and outlook conclude this thesis.

Chapter 3

The tree-level scattering amplitude

The goal of this thesis is to calculate non-perturbative effects in the amplitude for scattering the lightest flavor-octet of pseudoscalar (P) mesons off the lightest flavor-nonet of vector (V) mesons. The first step is to calculate the tree level amplitude for this process. For this purpose an effective field theory for the interaction is needed. This will be taken from [19] where the same process was studied in the presence of photons.

3.1 Introduction: QCD and Effective Theories

In the simplest quark model, a meson consists of a quark and an anti-quark, bound primarily by the strong interaction. According to quantum chromodynamics (QCD), the modern theory of the strong interaction, the dynamics of quarks and gluons follows from the Lagrangian density

$$\mathcal{L} = \bar{\psi}(i\not{D} - M)\psi - \frac{1}{4}G_{\mu\nu}^a G_a^{\mu\nu}, \quad (3.1)$$

with the gauge-covariant derivative

$$D^\mu = \partial^\mu + i g_s \lambda^a G_a^\mu, \quad (3.2)$$

where the λ 's are the Gell-Mann matrices and g_s is the strong coupling constant. The quark field ψ implicitly carries two indices, flavor and color.

3.1.1 Color

Color is the basic quantum number to which the gauge bosons, the gluons G_a^μ , couple. This is analogous to the photons which couple to the electric charge in Quantum electrodynamics. In contrast to QED, the quantum number color of the quark can take three different values; the symmetry group is not

U(1) but $SU(3)$. This is also the reason why there is an additional, quadratic contribution to the gluonic field strength tensor,

$$G_{\mu\nu}^a = \partial_\mu G_\nu^a - \partial_\nu G_\mu^a + g_s f^{abc} G_\mu^b G_\nu^c, \quad a = 1, \dots, 8, \quad (3.3)$$

where f^{abc} are the $SU(3)$ structure constants. In equ. (3.1) this last term gives rise to gluonic self-interactions.

The strong coupling constant g_s renormalized at high energies is small and a perturbative expansion is possible. For decreasing energy the coupling constant grows and perturbation theory breaks down. These two related effects, the self-interaction of the gluons and the large coupling constant at small energies lead to interesting phenomena. One of these is confinement: only color-neutral particles like mesons or baryons are observed in nature. Currently the Lagrangian (3.1) cannot be used directly to calculate bound states of quarks and gluons. Other methods have to be employed. One such method is Lattice gauge theory, which uses extensive numerical simulations. Another method is to consider the limit when N_c , the number of colors approaches infinity. In this special case some physical problems become easier to solve. The hope is that these relations still hold for the physical value $N_c = 3$. Higher order corrections should be suppressed by powers of $1/N_c$. This concept was first introduced to QCD by t' Hooft [20]. An introduction to large N_c QCD can be found in [21].

In this work, an interaction will be used that relies on large N_c QCD and another symmetry of the Lagrangian (3.1), flavor symmetry.

3.1.2 Flavor

Six different kinds of quarks or quark flavors are known. Three of them have masses of less than 1 GeV and will be considered in this work: the up, down and strange quark. The matrix M in the Lagrangian (3.1) contains the masses of these quarks. If the three quarks were massless, the QCD Lagrangian would be invariant under a transformation that mixes the quarks of different flavor. This would hold for both helicities of the quark separately and the Lagrangian density would have a $SU(3) \times SU(3)$ symmetry¹. This symmetry is broken in two ways. On the one hand the small but non-vanishing masses of the quarks break the symmetry explicitly. On the other hand this approximate symmetry $SU(3) \times SU(3)$ is spontaneously broken to $SU(3)$, as can be seen for example in the particle spectrum which only has the latter approximate symmetry. The theory of spontaneous symmetry breaking (as explained for example in [22]) claims that for every generator of an approximate global symmetry that is spontaneously broken, the spectrum must contain one approximately massless scalar particle with the quantum numbers of the generator. In the case at hand, these Goldstone bosons (GB)

¹Actually the symmetry group would be even larger, $U(3) \times U(3)$; the U(1) part adds further complications and will not be needed here.

are the lightest pseudoscalar mesons, the pion, the kaon and the eta. Furthermore at low energies an effective field theory can be used in which the GBs are the relevant degrees of freedom. This corresponds to an expansion in powers of small momenta and quark masses. In this chiral expansion, all terms that are consistent with the fundamental symmetries of the model, have to be considered. Power counting rules define an ordering scheme [23]. The zeroth order in this expansion vanishes.

3.2 The interaction

In [19], a combination of large N_c arguments and a chiral expansion to leading orders resulted in the following interaction density:

$$\begin{aligned}
\mathcal{L} = & f^2 \text{tr}\{U^\mu U_\mu^\dagger\} - \frac{1}{4} \text{tr}\{(D^\mu V_{\mu\alpha})(D_\nu V^{\nu\alpha})\} + \frac{1}{8} m_{1^-}^2 \text{tr}\{V^{\mu\nu} V_{\mu\nu}\} \\
& + i \frac{m_V h_V}{4} \text{tr}\{V_{\alpha\mu} V^{\mu\nu} V_\nu^\alpha\} + i \frac{\tilde{h}_V}{4 m_V} \text{tr}\{(D^\alpha V_{\alpha\mu}) V^{\mu\nu} (D^\beta V_{\beta\nu})\} \\
& + i \frac{h_A}{8} \epsilon^{\mu\nu\alpha\beta} \text{tr}\{(V_{\mu\nu} (D^\tau V_{\tau\alpha}) + (D^\tau V_{\tau\alpha}) V_{\mu\nu}) U_\beta\} \\
& + i \frac{m_V h_P}{2} \text{tr}\{U_\mu V^{\mu\nu} U_\nu\} + \frac{1}{4} g_D \text{tr}\{V^{\mu\nu} [V_{\mu\nu}, U_\alpha]_+ U^\alpha\} \\
& + \frac{1}{4} g_F \text{tr}\{V^{\mu\nu} [V_{\mu\nu}, U_\alpha]_- U^\alpha\} \\
& + \frac{1}{8} b_D \text{tr}\{V^{\mu\nu} V_{\mu\nu} \chi_+\} + i \frac{b_A}{8} \epsilon^{\mu\nu\alpha\beta} \text{tr}\{[V_{\mu\nu}, V_{\alpha\beta}]_+ \chi_-\}, \tag{3.4}
\end{aligned}$$

where the fields have the following particle content:

$$\begin{aligned}
V_{\mu\nu} &= \begin{pmatrix} \rho_{\mu\nu}^0 + \omega_{\mu\nu} & \sqrt{2} \rho_{\mu\nu}^+ & \sqrt{2} K_{\mu\nu}^+ \\ \sqrt{2} \rho_{\mu\nu}^- & -\rho_{\mu\nu}^0 + \omega_{\mu\nu} & \sqrt{2} K_{\mu\nu}^0 \\ \sqrt{2} K_{\mu\nu}^- & \sqrt{2} \bar{K}_{\mu\nu}^0 & \sqrt{2} \phi_{\mu\nu} \end{pmatrix}, \\
\Phi &= \begin{pmatrix} \pi^0 + \frac{1}{\sqrt{3}} \eta & \sqrt{2} \pi^+ & \sqrt{2} K^+ \\ \sqrt{2} \pi^- & -\pi^0 + \frac{1}{\sqrt{3}} \eta & \sqrt{2} K^0 \\ \sqrt{2} K^- & \sqrt{2} \bar{K}^0 & -\frac{2}{\sqrt{3}} \eta \end{pmatrix}. \tag{3.5}
\end{aligned}$$

The anti-symmetric tensor $\epsilon^{\mu\nu\alpha\beta}$ is given by

$$\begin{aligned}
\epsilon^{\mu\nu\alpha\beta} &= \begin{cases} +1 & \text{if } \mu, \nu, \alpha, \beta \text{ is an even permutation of } 0, 1, 2, 3 \\ -1 & \text{if } \mu, \nu, \alpha, \beta \text{ is an odd permutation of } 0, 1, 2, 3 \\ 0 & \text{otherwise} \end{cases}, \\
\epsilon^{\mu\nu\alpha\beta} &= -\epsilon_{\mu\nu\alpha\beta}. \tag{3.6}
\end{aligned}$$

The vector meson was represented by an anti-symmetric Lorentz tensor. This work will follow that convention. The isospin-averaged masses

$$\begin{aligned}
m_\pi &= 138 \text{ MeV}, & m_K &= 496 \text{ MeV}, & m_\eta &= 547 \text{ MeV}, \\
m_\rho &= 770 \text{ MeV}, & m_{K^*} &= 894 \text{ MeV}, & m_\omega &= 783 \text{ MeV}, & m_\phi &= 1019 \text{ MeV}, \tag{3.7}
\end{aligned}$$

will be used.

The other fields in the Lagrangian (3.4) are defined by

$$\begin{aligned}
\Gamma_\mu &= \frac{1}{2} (u^\dagger \partial_\mu u + u \partial_\mu u^\dagger), & u &= \exp\left(\frac{i\Phi}{2f}\right), \\
U_\mu &= \frac{1}{2} u^\dagger (\partial_\mu e^{i\frac{\Phi}{f}}) u^\dagger = \frac{i\partial_\mu \Phi}{2f} + \mathcal{O}(\Phi^2), \\
D_\mu V_{\alpha\beta} &= \partial_\mu V_{\alpha\beta} + [\Gamma_\mu, V_{\alpha\beta}] = \partial_\mu V_{\alpha\beta} + \frac{1}{8f^2} [[\Phi, \partial_\mu \Phi], V_{\alpha\beta}] + \mathcal{O}(\Phi^3), \\
\chi_+ &= \frac{1}{2} u \chi_0 u + \frac{1}{2} u^\dagger \chi_0 u^\dagger = \chi_0 - \frac{1}{8f^2} \{ \{ \chi_0, \Phi \}, \Phi \} + \mathcal{O}(\Phi^3), \\
\chi_- &= \frac{1}{2} u \chi_0 u - \frac{1}{2} u^\dagger \chi_0 u^\dagger = \frac{i}{2f} \{ \Phi, \chi_0 \} + \mathcal{O}(\Phi^3), \\
\chi_0 &= \begin{pmatrix} m_\pi^2 & 0 & 0 \\ 0 & m_\pi^2 & 0 \\ 0 & 0 & 2m_K^2 - m_\pi^2 \end{pmatrix}, \tag{3.8}
\end{aligned}$$

which guarantees an interaction in agreement with the constraints from chiral symmetry, see e.g. [24, 23].

Most coupling constants in the Lagrangian (3.4) were already derived in [19]. The mass splitting within the vector meson multiplet leads to an estimate of $b_D = 0.92 \pm 0.05$. h_P was calculated from the vector meson decays $\rho \rightarrow \pi\pi$, $\phi \rightarrow \bar{K}K$ and $K^* \rightarrow \pi K$ as $h_P = 0.29 \pm 0.03$. The values h_V and \tilde{h}_V were estimated from the magnetic moment and the quadrupole moment of the vector mesons. Finally the radiative decays $K_\pm^* \rightarrow K_\pm \gamma$, $K_0^* \rightarrow K_0 \gamma$ and $\phi \rightarrow \eta \gamma$ led to the values for h_A and b_A . In this work the following values will be used:

$$\begin{aligned}
h_P &= 0.29, & h_A &= 2.10, & b_A &= 0.27, & m_V &= 776 \text{ MeV}, \\
h_V &= 0.45, & \tilde{h}_V &= 3.72, & b_D &= 0.92, & f_\pi &= 90 \text{ MeV}. \tag{3.9}
\end{aligned}$$

The other constants g_D and g_F will be used to fit the results to the measured spectrum.

At leading order the interaction (3.4) results in a total of 16 diagrams that contribute: four contact interactions, a pseudoscalar s - and u -channel exchange and a total of ten vector exchange processes. A straight-forward calculation of the tree level scattering amplitude leads to

$$\begin{aligned}
T_{\text{tree}}^{\bar{\mu}\bar{\nu},\mu\nu}(\bar{q}, \bar{p}; q, p) &= -\frac{C_{WT}}{4f_\pi^2} g^{\bar{\nu}\nu} (p^\mu (q + \bar{q})^{\bar{\mu}} + \bar{p}^{\bar{\mu}} (q + \bar{q})^\mu) \\
&- \frac{1}{16f^2} g^{\bar{\mu}\mu} g^{\bar{\nu}\nu} \{ (C_D g_D + C_F g_F) (q \cdot \bar{q}) + C_\chi b_D \} \\
&- \sum_{x \in [8]} C_{s\text{-ch}}^{(x)} \left(\frac{m_V h_P}{2f^2} \right)^2 \bar{p}^{\bar{\mu}} \bar{q}^{\bar{\nu}} S_x(p + q) p^\mu q^\nu
\end{aligned}$$

$$\begin{aligned}
& - \sum_{x \in [8]} C_{u-ch}^{(x)} \left(\frac{m_V h_P}{2 f^2} \right)^2 \bar{p}^{\bar{\mu}} q^{\bar{\nu}} S_x(p - \bar{q}) p^\mu \bar{q}^\nu \\
& - \sum_{x \in [9]} C_{s-ch}^{(11,x)} \frac{h_A^2}{16 f^2} \Gamma_{\bar{\alpha}\bar{\beta}}^{\bar{\mu}\bar{\nu}}(\bar{p}, \bar{q}) S_x^{\bar{\alpha}\bar{\beta}, \alpha\beta}(p + q) \Gamma_{\alpha\beta}^{\mu\nu}(p, q) \\
& - \sum_{x \in [9]} \frac{h_A b_A}{8 f^2} \left\{ C_{s-ch}^{(12,x)} \Gamma_{\bar{\alpha}\bar{\beta}}^{\bar{\mu}\bar{\nu}}(\bar{p}, \bar{q}) S_x^{\bar{\alpha}\bar{\beta}, \alpha\beta}(p + q) \epsilon^{\mu\nu}_{\alpha\beta} \right. \\
& \quad \left. + C_{s-ch}^{(21,x)} \epsilon^{\bar{\mu}\bar{\nu}}_{\bar{\alpha}\bar{\beta}} S_x^{\bar{\alpha}\bar{\beta}, \alpha\beta}(p + q) \Gamma_{\alpha\beta}^{\mu\nu}(p, q) \right\} \\
& - \sum_{x \in [9]} C_{s-ch}^{(22,x)} \frac{b_A^2}{4 f^2} \epsilon^{\bar{\mu}\bar{\nu}}_{\bar{\alpha}\bar{\beta}} S_x^{\bar{\alpha}\bar{\beta}, \alpha\beta}(p + q) \epsilon^{\mu\nu}_{\alpha\beta} \\
& - \sum_{x \in [9]} C_{u-ch}^{(11,x)} \frac{h_A^2}{16 f^2} \Gamma_{\bar{\alpha}\bar{\beta}}^{\bar{\mu}\bar{\nu}}(\bar{p}, -q) S_x^{\bar{\alpha}\bar{\beta}, \alpha\beta}(p - \bar{q}) \Gamma_{\alpha\beta}^{\mu\nu}(p, -\bar{q}) \\
& - \sum_{x \in [9]} \frac{h_A b_A}{8 f^2} \left\{ C_{u-ch}^{(12,x)} \Gamma_{\bar{\alpha}\bar{\beta}}^{\bar{\mu}\bar{\nu}}(\bar{p}, -q) S_x^{\bar{\alpha}\bar{\beta}, \alpha\beta}(p - \bar{q}) \epsilon^{\mu\nu}_{\alpha\beta} \right. \\
& \quad \left. + C_{u-ch}^{(21,x)} \epsilon^{\bar{\mu}\bar{\nu}}_{\bar{\alpha}\bar{\beta}} S_x^{\bar{\alpha}\bar{\beta}, \alpha\beta}(p - \bar{q}) \Gamma_{\alpha\beta}^{\mu\nu}(p, -\bar{q}) \right\} \\
& - \sum_{x \in [9]} C_{u-ch}^{(22,x)} \frac{b_A^2}{4 f^2} \epsilon^{\bar{\mu}\bar{\nu}}_{\bar{\alpha}\bar{\beta}} S_x^{\bar{\alpha}\bar{\beta}, \alpha\beta}(p - \bar{q}) \epsilon^{\mu\nu}_{\alpha\beta} \\
& + \sum_{x \in [9]} C_{t-ch}^{(x)} \frac{h_P}{2 f^2} \bar{q}_{\bar{\alpha}} q_{\bar{\beta}} S_a^{\bar{\alpha}\bar{\beta}, \alpha\beta}(\bar{q} - q) \left\{ 3 m_V^2 h_V g_{\alpha}^{\bar{\mu}} g_{\beta}^{\mu} g^{\bar{\nu}\nu} \right. \\
& \quad \left. + \tilde{h}_V \left[g_{\alpha}^{\bar{\nu}} g_{\beta}^{\nu} \bar{p}^{\bar{\mu}} p^{\mu} + g_{\beta}^{\bar{\nu}} g^{\bar{\mu}\nu} p^{\mu} (p - \bar{p})_{\alpha} - g^{\bar{\nu}\nu} g_{\beta}^{\mu} (p - \bar{p})_{\alpha} \bar{p}^{\bar{\mu}} \right] \right\},
\end{aligned}$$

$$\Gamma_{\alpha\beta}^{\mu\nu}(p, q) = q^{\gamma} (p + q)_{\alpha} \varepsilon^{\mu\nu}_{\beta\gamma} + q^{\gamma} p^{\mu} \varepsilon_{\alpha}^{\nu}_{\beta\gamma}. \quad (3.10)$$

Some comments about the notation are in order: p and \bar{p} are the incoming and outgoing vector meson momenta while q and \bar{q} are the momenta of the pseudoscalar mesons. The total momentum is $w = p + q = \bar{p} + \bar{q}$. The summation index x runs over the exchanged particles, either the octet of Goldstone Bosons or the nonet of vector mesons. The propagators are given by

$$\begin{aligned}
S_x(p) &= \frac{1}{p^2 - m_x^2 + i\epsilon}, \\
S_x^{\mu\nu, \alpha\beta}(p) &= -\frac{1}{m_x^2} \frac{1}{p^2 - m_x^2 + i\epsilon} \left[(m_x^2 - p^2) g^{\mu\alpha} g^{\nu\beta} \right. \\
& \quad \left. + g^{\mu\alpha} p^{\nu} p^{\beta} - g^{\mu\beta} p^{\nu} p^{\alpha} - (\mu \leftrightarrow \nu) \right]. \quad (3.11)
\end{aligned}$$

A list with all coupled channels considered in this work is given in table 3.1. The prefactors C in equ. (3.10) follow from the group structure of the interaction and detail the strength of the interaction among the coupled

$(0, 2)$	$(1, 2)$	$(\frac{1}{2}, 1)$
$(\frac{i}{\sqrt{2}} K_{\mu\nu}^t \sigma_2 K)$	$(\frac{i}{\sqrt{2}} K_{\mu\nu}^t \sigma_2 \vec{\sigma} K)$	$(\frac{1}{\sqrt{3}} \pi \cdot \sigma K_{\mu\nu})$ $(\frac{1}{\sqrt{3}} \rho_{\mu\nu} \cdot \sigma K)$ $(\omega_{\mu\nu} K)$ $(\eta K_{\mu\nu})$ $(\phi_{\mu\nu} K)$
$(\frac{3}{2}, 1)$	$(0^+, 0)$	$(0^-, 0)$
$(\pi \cdot T K_{\mu\nu})$ $(\rho_{\mu\nu} \cdot T K)$	$\frac{1}{2} (\bar{K} K_{\mu\nu} - \bar{K}_{\mu\nu} K)$	$(\frac{1}{\sqrt{3}} \rho_{\mu\nu} \cdot \pi)$ $(\omega_{\mu\nu} \eta)$ $\frac{1}{2} (\bar{K} K_{\mu\nu} + \bar{K}_{\mu\nu} K)$ $(\phi_{\mu\nu} \eta)$
$(1^+, 0)$	$(1^-, 0)$	$(2, 0)$
$(\vec{\pi} \omega_{\mu\nu})$ $(\vec{\pi} \phi_{\mu\nu})$ $(\vec{\rho}_{\mu\nu} \eta)$ $\frac{1}{2} (\bar{K} \vec{\sigma} K_{\mu\nu} + \bar{K}_{\mu\nu} \vec{\sigma} K)$	$-\frac{i}{\sqrt{2}} (\vec{\rho}_{\mu\nu} \times \vec{\pi})$ $\frac{1}{2} (\bar{K} \vec{\sigma} K_{\mu\nu} - \bar{K}_{\mu\nu} \vec{\sigma} K)$	$\frac{1}{2} (\pi^i \rho_{\mu\nu}^j + \pi^j \rho_{\mu\nu}^i) - \frac{1}{3} \delta^{ij} \pi \cdot \rho_{\mu\nu}$

Table 3.1: Coupled-channel states (I^G, S) , with isospin (I), G-parity (G) and strangeness (S).

channels; they are given in the tables (3.2-3.6). The s -channel coefficients are listed in a factorized form:

$$[C_{s-ch}^{(x)}]_{ab} = G_a^{(x)} G_b^{(x)}, \quad [C_{s-ch}^{(ij,x)}]_{ab} = G_a^{(i,x)} G_b^{(j,x)}. \quad (3.12)$$

3.3 Partial wave projection

The next step is a partial wave expansion of the tree-level amplitude (3.10) as demonstrated in the appendix of [15]. To summarize this appendix briefly: once the amplitudes G_i fulfilling

$$\begin{aligned}
\langle \bar{\lambda} | T | \lambda \rangle &\equiv \epsilon_{\bar{\mu}\bar{\nu}}^\dagger(\bar{p}, \bar{\lambda}) T_{\text{tree}}^{\bar{\mu}\bar{\nu}, \mu\nu} \epsilon_{\mu\nu}(p, \lambda) \\
&= \epsilon_{\bar{\mu}}^\dagger(\bar{p}, \bar{\lambda}) \left\{ G_1 g^{\bar{\mu}\mu} + G_2 w^{\bar{\mu}} w^\mu \right. \\
&\quad \left. + G_3 w^{\bar{\mu}} \bar{p}^\mu + G_4 p^{\bar{\mu}} w^\mu + G_5 p^{\bar{\mu}} \bar{p}^\mu \right\} \epsilon_\mu(p, \lambda), \quad (3.13)
\end{aligned}$$

(a)	$[G_{(1^+,0)}^{(1,\rho)}]_a$	$[G_{(1^+,0)}^{(2,\rho)}]_a$	$[G_{(0^-,0)}^{(1,\omega)}]_a$	$[G_{(0^-,0)}^{(2,\omega)}]_a$	$[G_{(0^-,0)}^{(1,\phi)}]_a$	$[G_{(0^-,0)}^{(2,\phi)}]_a$
(1)	1	$2 m_\pi^2$	$\sqrt{3}$	$\sqrt{3} 2 m_\pi^2$	0	0
(2)	0	0	$\frac{1}{\sqrt{3}}$	$\frac{2}{\sqrt{3}} m_\pi^2$	0	0
(3)	$\frac{1}{\sqrt{3}}$	$\frac{2}{\sqrt{3}} m_\pi^2$	1	$2 m_K^2$	$\sqrt{2}$	$\sqrt{8} m_K^2$
(4)	1	$2 m_K^2$	0	0	$-\frac{2}{\sqrt{3}}$	$\frac{4}{\sqrt{3}} m_\pi^2 - \frac{8}{\sqrt{3}} m_K^2$
(a)	$[G_{(1^-,0)}^{(\pi)}]_a$	$[G_{(0^+,0)}^{(\eta)}]_a$	$[G_{(\frac{1}{2},1)}^{(K)}]_a$		$[G_{(\frac{1}{2},1)}^{(1,K^*)}]_a$	$[G_{(\frac{1}{2},1)}^{(2,K^*)}]_a$
(1)	$\sqrt{2}$	$\sqrt{3}$	$\frac{\sqrt{3}}{2}$		$\frac{\sqrt{3}}{2}$	$\sqrt{3} m_\pi^2$
(2)	1	—	$-\frac{\sqrt{3}}{2}$		$\frac{\sqrt{3}}{2}$	$\sqrt{3} m_K^2$
(3)	—	—	$-\frac{1}{2}$		$\frac{1}{2}$	m_K^2
(4)	—	—	$\frac{\sqrt{3}}{2}$		$-\frac{1}{2\sqrt{3}}$	$\sqrt{3} m_\pi^2 - \frac{4}{\sqrt{3}} m_K^2$
(5)	—	—	$\frac{1}{\sqrt{2}}$		$\frac{1}{\sqrt{2}}$	$\sqrt{2} m_K^2$

Table 3.2: Coupling constants specifying the s-channel meson exchange contributions (see (3.12)).

are known, the partial-wave projection can be written down.²

Additional Lorentz structures containing p^μ or \bar{p}^μ do not contribute in equ. (3.13) since they vanish when contracted with the polarization vectors. The latter can be transformed between vector and tensor representation by

$$\epsilon_{\mu\nu}(p, \lambda) = \frac{i}{\sqrt{p^2}} \left\{ p_\mu \epsilon_\nu(p, \lambda) - p_\nu \epsilon_\mu(p, \lambda) \right\}. \quad (3.14)$$

The convention used for the polarization vectors is

$$\epsilon_\mu(p) = \begin{pmatrix} 0 \\ \frac{\pm 1}{\sqrt{2}} \\ \frac{-i}{\sqrt{2}} \\ 0 \end{pmatrix}, \quad \begin{pmatrix} \frac{p_{cm}}{M} \\ 0 \\ 0 \\ \frac{\omega}{M} \end{pmatrix}, \quad \epsilon_\mu(\bar{p}) = \begin{pmatrix} 0 \\ \frac{\mp \cos \Theta}{\sqrt{2}} \\ \frac{-i}{\sqrt{2}} \\ \frac{\pm \sin \Theta}{\sqrt{2}} \end{pmatrix}, \quad \begin{pmatrix} \frac{p_{cm}}{M} \\ \frac{\omega}{M} \sin \Theta \\ 0 \\ \frac{\omega}{M} \cos \Theta \end{pmatrix}, \quad (3.15)$$

with $\epsilon_\mu(p) = \epsilon_\mu(p, \pm 1)$, $\epsilon(\bar{p}, 0)$, $\epsilon_\mu(\bar{p}) = \epsilon_\mu(\bar{p}, \pm 1)$, $\epsilon(\bar{p}, 0)$ and the further definitions $\omega^2 = M^2 + p_{cm}^2$ and $\bar{\omega}^2 = \bar{M}^2 + \bar{p}_{cm}^2$.

(Using equ. (3.14) in equ. (3.13) determines how to transform the scattering amplitude between vector and tensor representation:

$$T_{\text{tree}}^{\bar{\mu}, \mu} = \frac{\bar{p}_\nu}{M} \left(T_{\text{tree}}^{\bar{\mu}\bar{\nu}, \mu\nu} - T_{\text{tree}}^{\bar{\nu}\bar{\mu}, \mu\nu} - T_{\text{tree}}^{\bar{\mu}\bar{\nu}, \nu\mu} + T_{\text{tree}}^{\bar{\nu}\bar{\mu}, \nu\mu} \right) \frac{p_\nu}{M}. \quad (3.16)$$

The transformations of the scattering amplitude in the equation above and in the polarization vectors in equ. (3.14) in principle reduce the problem to the situation in the appendix of [15] where only the vector representation was used.)

²The basis of Lorentz structures multiplying the G_i in equ. (3.13) differs from the one chosen in [15] by a change of basis which is straight-forward to implement.

(I, S)	ch	C_{t-ch}^ρ	$C_{u-ch}^{11,\rho}$	$C_{u-ch}^{12,\rho}$	$C_{u-ch}^{21,\rho}$	$C_{u-ch}^{22,\rho}$	C_{u-ch}^π
$(0, 2)$	11	$\frac{3}{4}$	$\frac{3}{4}$	$\frac{3}{2} m_K^2$	$\frac{3}{2} m_K^2$	$3 m_K^4$	$\frac{3}{4}$
$(1, 2)$	11	$-\frac{1}{4}$	$\frac{1}{4}$	$\frac{1}{2} m_K^2$	$\frac{1}{2} m_K^2$	m_K^4	$\frac{1}{4}$
$(\frac{1}{2}, 1)$	11	1	0	0	0	0	0
	12	0	0	0	0	0	-1
	13	0	$\frac{\sqrt{3}}{2}$	$\sqrt{3} m_\pi^2$	$\sqrt{3} m_K^2$	$2\sqrt{3} m_\pi^2 m_K^2$	0
	22	1	0	0	0	0	0
	24	0	$\frac{1}{2}$	m_K^2	m_π^2	$2 m_\pi^2 m_K^2$	0
$(\frac{3}{2}, 1)$	11	$-\frac{1}{2}$	0	0	0	0	0
	12	0	0	0	0	0	$\frac{1}{2}$
	22	$-\frac{1}{2}$	0	0	0	0	0
$(0^+, 0)$	11	$\frac{3}{4}$	$-\frac{3}{4}$	$-\frac{3}{2} m_K^2$	$-\frac{3}{2} m_K^2$	$-3 m_K^4$	$\frac{3}{4}$
$(0^-, 0)$	11	2	0	0	0	0	-2
	12	0	1	$2 m_\pi^2$	$2 m_\pi^2$	$4 m_\pi^4$	0
	33	$\frac{3}{4}$	$\frac{3}{4}$	$\frac{3}{2} m_K^2$	$\frac{3}{2} m_K^2$	$3 m_K^4$	$-\frac{3}{4}$
$(1^+, 0)$	11	0	1	$2 m_\pi^2$	$2 m_\pi^2$	$4 m_\pi^4$	0
	33	0	$\frac{1}{3}$	$\frac{2}{3} m_\pi^2$	$\frac{2}{3} m_\pi^2$	$\frac{4}{3} m_\pi^4$	0
	44	$-\frac{1}{4}$	$-\frac{1}{4}$	$-\frac{1}{2} m_K^2$	$-\frac{1}{2} m_K^2$	$-m_K^4$	$\frac{1}{4}$
$(1^-, 0)$	11	1	0	0	0	0	1
	22	$-\frac{1}{4}$	$\frac{1}{4}$	$\frac{1}{2} m_K^2$	$\frac{1}{2} m_K^2$	m_K^4	$-\frac{1}{4}$
$(2, 0)$	11	-1	0	0	0	0	1

Table 3.3: Coupling constants specifying the interaction strength as defined in (3.10).

(I, S)	ch	C_{t-ch}^ω	$C_{u-ch}^{11,\omega}$	$C_{u-ch}^{12,\omega}$	$C_{u-ch}^{21,\omega}$	$C_{u-ch}^{22,\omega}$	C_{u-ch}^η
$(0, 2)$	11	$-\frac{1}{4}$	$-\frac{1}{4}$	$-\frac{1}{2}m_K^2$	$-\frac{1}{2}m_K^2$	$-m_K^4$	$-\frac{3}{4}$
$(1, 2)$	11	$-\frac{1}{4}$	$\frac{1}{4}$	$\frac{1}{2}m_K^2$	$\frac{1}{2}m_K^2$	m_K^4	$\frac{3}{4}$
$(\frac{1}{2}, 1)$	12	0	$\frac{1}{2}$	m_π^2	m_K^2	$2m_K^4m_\pi^4$	0
	34	0	$\frac{1}{2\sqrt{3}}$	$\frac{1}{\sqrt{3}}m_K^2$	$\frac{1}{\sqrt{3}}m_\pi^2$	$\frac{2}{\sqrt{3}}m_K^2m_\pi^2$	0
$(\frac{3}{2}, 1)$	12	0	$\frac{1}{2}$	m_π^2	m_K^2	$2m_K^2m_\pi^2$	0
$(0^+, 0)$	11	$\frac{1}{4}$	$-\frac{1}{4}$	$-\frac{1}{2}m_K^2$	$-\frac{1}{2}m_K^2$	$-m_K^4$	$\frac{3}{4}$
$(0^-, 0)$	11	0	1	$2m_\pi^2$	$2m_\pi^2$	$4m_\pi^4$	0
	22	0	$\frac{1}{3}$	$\frac{2}{3}m_\pi^2$	$\frac{2}{3}m_\pi^2$	$\frac{4}{3}m_\pi^4$	0
	33	$\frac{1}{4}$	$\frac{1}{4}$	$\frac{1}{2}m_K^2$	$\frac{1}{2}m_K^2$	m_K^4	$-\frac{3}{4}$
$(1^+, 0)$	13	0	$\frac{1}{\sqrt{3}}$	$\frac{2}{\sqrt{3}}m_\pi^2$	$\frac{2}{\sqrt{3}}m_\pi^2$	$\frac{4}{\sqrt{3}}m_\pi^4$	0
	44	$\frac{1}{4}$	$\frac{1}{4}$	$\frac{1}{2}m_K^2$	$\frac{1}{2}m_K^2$	m_K^4	$-\frac{3}{4}$
$(1^-, 0)$	11	0	-1	$-2m_\pi^2$	$-2m_\pi^2$	$-4m_\pi^4$	0
	22	$\frac{1}{4}$	$-\frac{1}{4}$	$-\frac{1}{2}m_K^2$	$-\frac{1}{2}m_K^2$	$-m_K^4$	$\frac{3}{4}$
$(2, 0)$	11	0	1	$2m_\pi^2$	$2m_\pi^2$	$4m_\pi^4$	0

Table 3.4: Coupling constants specifying the interaction strength as defined in (3.10) continued.

(I, S)	ch	$C_{t-ch}^{K^*}$	C_{u-ch}^{11,K^*}	C_{u-ch}^{12,K^*}	C_{u-ch}^{21,K^*}	C_{u-ch}^K
$(\frac{1}{2}, 1)$	11	0	$-\frac{1}{4}$	$-\frac{1}{2}m_\pi^2$	$-\frac{1}{2}m_\pi^2$	$-\frac{1}{4}$
	12	$\frac{1}{4}$	0	0	0	0
	13	$-\frac{\sqrt{3}}{4}$	0	0	0	0
	14	0	$-\frac{1}{4}$	$-\frac{1}{2}m_\pi^2$	$\frac{3}{2}m_\pi^2 - 2m_K^2$	$\frac{3}{4}$
	15	$\sqrt{\frac{3}{8}}$	0	0	0	0
	22	0	$-\frac{1}{4}$	$-\frac{1}{2}m_K^2$	$-\frac{1}{2}m_K^2$	$-\frac{1}{4}$
	23	0	$\frac{\sqrt{3}}{4}$	$\frac{\sqrt{3}}{2}m_K^2$	$\frac{\sqrt{3}}{2}m_K^2$	$\frac{\sqrt{3}}{4}$
	24	$-\frac{3}{4}$	0	0	0	0
	25	0	$\sqrt{\frac{3}{8}}$	$\sqrt{\frac{3}{2}}m_K^2$	$\sqrt{\frac{3}{2}}m_K^2$	$-\sqrt{\frac{3}{8}}$
	33	0	$\frac{1}{4}$	$\frac{1}{2}m_K^2$	$\frac{1}{2}m_K^2$	$\frac{1}{4}$
	34	$-\frac{\sqrt{3}}{4}$	0	0	0	0
	35	0	$\frac{1}{\sqrt{8}}$	$\frac{1}{\sqrt{2}}m_K^2$	$\frac{1}{\sqrt{2}}m_K^2$	$-\frac{1}{\sqrt{8}}$
	44	0	$\frac{1}{12}$	$\frac{2}{3}m_K^2 - \frac{1}{2}m_\pi^2$	$\frac{2}{3}m_K^2 - \frac{1}{2}m_\pi^2$	$\frac{3}{4}$
	45	$\sqrt{\frac{3}{8}}$	0	0	0	0
	55	0	$\frac{1}{2}$	m_K^2	m_K^2	$\frac{1}{2}$
$(\frac{3}{2}, 1)$	11	0	$\frac{1}{2}$	m_π^2	m_π^2	$\frac{1}{2}$
	12	$-\frac{1}{2}$	0	0	0	0
	22	0	$\frac{1}{2}$	m_K^2	m_K^2	$\frac{1}{2}$
$(0^-, 0)$	13	$\frac{\sqrt{3}}{2}$	$\frac{\sqrt{3}}{2}$	$\sqrt{3}m_\pi^2$	$\sqrt{3}m_K^2$	$-\frac{\sqrt{3}}{2}$
	23	$\frac{\sqrt{3}}{2}$	$-\frac{1}{2\sqrt{3}}$	$\sqrt{3}m_\pi^2 - \frac{4}{\sqrt{3}}m_K^2$	$-\frac{1}{\sqrt{3}}m_K^2$	$-\frac{\sqrt{3}}{2}$
	34	$-\sqrt{\frac{3}{2}}$	$-\frac{1}{\sqrt{6}}$	$-\sqrt{\frac{2}{3}}m_K^2$	$\sqrt{6}m_\pi^2 - \frac{4\sqrt{6}}{3}m_K^2$	$\sqrt{\frac{3}{2}}$
$(1^+, 0)$	14	$\frac{1}{2}$	$\frac{1}{2}$	m_π^2	m_K^2	$-\frac{1}{2}$
	24	$-\frac{1}{\sqrt{2}}$	$\frac{1}{\sqrt{2}}$	$\sqrt{2}m_\pi^2$	$\sqrt{2}m_K^2$	$\frac{1}{\sqrt{2}}$
	34	$\frac{\sqrt{3}}{2}$	$-\frac{1}{2\sqrt{3}}$	$\sqrt{3}m_\pi^2 - \frac{4}{\sqrt{3}}m_K^2$	$-\frac{1}{\sqrt{3}}m_K^2$	$-\frac{\sqrt{3}}{2}$
$(1^-, 0)$	12	$\frac{1}{\sqrt{2}}$	$-\frac{1}{\sqrt{2}}$	$-\sqrt{2}m_\pi^2$	$-\sqrt{2}m_K^2$	$\frac{1}{\sqrt{2}}$

Table 3.5: Coupling constants specifying the interaction strength as defined in (3.10) continued. The coefficients C_{u-ch}^{22,K^*} are not displayed. They obey the relation $C_{u-ch}^{22,K^*} = C_{u-ch}^{12,K^*} \cdot C_{u-ch}^{21,K^*} / C_{u-ch}^{11,K^*}$

(I^G, S)	ch	C_{t-ch}^ϕ	$C_{u-ch}^{11,\phi}$	$C_{u-ch}^{12,\phi}$	$C_{u-ch}^{21,\phi}$
(0, 2)	11	$-\frac{1}{2}$	$-\frac{1}{2}$	$-m_K^2$	$-m_K^2$
(1, 2)	11	$-\frac{1}{2}$	$\frac{1}{2}$	m_K^2	m_K^2
$(\frac{1}{2}, 1)$	45	0	$-\sqrt{\frac{2}{3}}$	$-\frac{4\sqrt{6}}{3}m_K^2 + \frac{2\sqrt{6}}{3}m_\pi^2$	$-\sqrt{\frac{8}{3}}m_K^2$
$(0^+, 0)$	11	$\frac{1}{2}$	$-\frac{1}{2}$	$-m_K^2$	$-m_K^2$
$(0^-, 0)$	33	$\frac{1}{2}$	$\frac{1}{2}$	m_K^2	m_K^2
	44	0	$\frac{4}{3}$	$\frac{16}{3}m_K^2 - \frac{8}{3}m_\pi^2$	$\frac{16}{3}m_K^2 - \frac{8}{3}m_\pi^2$
$(1^+, 0)$	44	$\frac{1}{2}$	$\frac{1}{2}$	m_K^2	m_K^2
$(1^-, 0)$	22	$\frac{1}{2}$	$-\frac{1}{2}$	$-m_K^2$	$-m_K^2$

Table 3.6: Coupling constants specifying the interaction strength as defined in (3.10) continued. The coefficients $C_{u-ch}^{22,\phi}$ are not displayed. They obey the relation $C_{u-ch}^{22,\phi} = C_{u-ch}^{12,\phi} \cdot C_{u-ch}^{21,\phi} / C_{u-ch}^{11,\phi}$

In the next step partial wave amplitudes are introduced in the center of mass frame,

$$\epsilon_{\bar{\mu}\bar{\nu}}^\dagger(\bar{p}, \bar{\lambda}) T_{\text{tree}}^{\bar{\mu}\bar{\nu}, \mu\nu} \epsilon_{\mu\nu}(p, \lambda) = \sum_J (2J+1) \langle \bar{\lambda} | T^{(J)} | \lambda \rangle d_{\lambda\bar{\lambda}}^{(J)}(\Theta), \quad (3.17)$$

where $d_{\lambda\bar{\lambda}}^{(J)}(\Theta)$ denote Wigner's rotation functions and Θ is the angle spanned by the incoming and outgoing vector meson three-momentum³. In the center of mass frame the left hand side of this equation can be calculated explicitly in terms of the invariant amplitudes G_i using the right hand side of equ. (3.13) and the expressions in equ. (3.15) for the polarization tensors.

If the G_i are known, the objects

$$\langle \bar{\lambda} | T^{(J)} | \lambda \rangle = \int_{-1}^1 \frac{d \cos \Theta}{2} \langle \bar{\lambda} | T | \lambda \rangle d_{\lambda\bar{\lambda}}^{(J)}, \quad (3.18)$$

are now accessible. These are the desired objects, but in a different basis. The transformation of basis consists of several steps.

In the first step, the previous equation is rewritten in terms of parity eigenstates which are defined by:

$$\begin{aligned} \langle 1_\pm | &= (\pm \langle +1 | + \langle -1 |) / \sqrt{2}, \\ \langle 2_+ | &= \langle 0 |. \end{aligned} \quad (3.19)$$

The second step is almost trivial for negative parity. There is just one state in equ. (3.18). The corresponding one-dimensional matrix will be rescaled

³In [15] there is an ambiguity in the definition of that angle. If $p \cdot \bar{p} = \omega \bar{\omega} - \cos(\Theta) p_{cm} \bar{p}_{cm}$ holds, the sign of F_3 and F_4 has to be changed.

by a factor $1/(p_{cm}\bar{p}_{cm})^J$. For positive parity the two by two matrix in equ. (3.18) is multiplied from the right by

$$\frac{U}{p_{cm}^J} = \frac{1}{p_{cm}^J} \begin{pmatrix} \frac{1}{p_{cm}} & -\sqrt{\frac{J}{J+1}} \frac{\omega}{M p_{cm}} \\ 0 & \frac{1}{M p_{cm}} \end{pmatrix}, \quad (3.20)$$

and from the left by

$$\frac{\bar{U}^T}{\bar{p}_{cm}^J}, \quad \bar{U} = U(p_{cm} \leftrightarrow \bar{p}_{cm}, \omega \leftrightarrow \bar{\omega}, M \leftrightarrow \bar{M}). \quad (3.21)$$

Those steps above will lead to the invariant amplitudes M listed in the appendix of [15]. There is an additional freedom that will be used in this work. The resulting invariant amplitudes can be rescaled with a power of $s = (p+q)^2$ if the phase space (to be introduced in the next chapter) is rescaled with the inverse expression. For positive parity the following exponents will be used:

$$T_{i,j}^{(1+)} = s^{d_{i,j}} M_{i,j}^{(1+)}, \quad d_{1,1} = 1, \quad d_{1,2} = d_{2,1} = \frac{3}{2}, \quad d_{2,2} = 2. \quad (3.22)$$

In this work only positive parity and angular momentum one, $J = 1$ is considered. The final expression is

$$\begin{aligned} T_{11}^{(1+)} &= \int_{-1}^1 \frac{dx}{2} \left\{ -\frac{1+x^2}{2} s G_1 + \frac{x^3-x}{2} \bar{p}_{cm} p_{cm} s G_5 \right\}, \\ T_{12}^{(1+)} &= \int_{-1}^1 \frac{dx}{2} \left\{ \frac{3x^2-1}{\sqrt{8}} \frac{\omega s^{\frac{3}{2}}}{p_{cm}^2} G_1 \right. \\ &\quad \left. + s^2 \frac{x^2-1}{\sqrt{2}} G_4 \right. \\ &\quad \left. + \frac{s^{3/2}(1-x^2)}{\sqrt{8} p_{cm}} (3\omega \bar{p}_{cm} x - 2\bar{\omega} p_{cm}) G_5 \right\}, \\ T_{21}^{(1+)} &= \int_{-1}^1 \frac{dx}{2} \left\{ \frac{3x^2-1}{\sqrt{8}} \frac{\bar{\omega} s^{\frac{3}{2}}}{\bar{p}_{cm}^2} G_1 \right. \\ &\quad \left. + s^2 \frac{x^2-1}{\sqrt{2}} G_3 \right. \\ &\quad \left. + \frac{s^{3/2}(1-x^2)}{\sqrt{8} \bar{p}_{cm}} (3\bar{\omega} p_{cm} x - 2\omega \bar{p}_{cm}) G_5 \right\}, \\ T_{22}^{(1+)} &= \int_{-1}^1 \frac{dx}{2} \left\{ \frac{s^2}{4 p_{cm}^2 \bar{p}_{cm}^2} (4x p_{cm} \bar{p}_{cm} + \omega \bar{\omega} (3-9x^2)) G_1 \right. \\ &\quad \left. + \frac{s^3 x}{p_{cm} \bar{p}_{cm}} G_2 \right. \\ &\quad \left. + s^{5/2} \frac{2\bar{\omega} x p_{cm} + \omega \bar{p}_{cm} (1-3x^2)}{2 p_{cm}^2 \bar{p}_{cm}} G_3 \right\} \end{aligned}$$

$$\begin{aligned}
& + s^{5/2} \frac{2\omega x \bar{p}_{cm} + \bar{\omega} p_{cm}(1-3x^2)}{2p_{cm}\bar{p}_{cm}^2} G_4 \\
& + \frac{s^2}{4p_{cm}^2\bar{p}_{cm}^2} \left[2(1-3x^2) \cdot (\omega^2\bar{p}_{cm}^2 + \bar{\omega}^2 p_{cm}^2) \right. \\
& \left. + x p_{cm} \bar{p}_{cm} \omega \bar{\omega} (9x^2 - 1) \right] G_5 \}, \tag{3.23}
\end{aligned}$$

with $x = \cos(\Theta)$ and the usual Mandelstam variables

$$s = (p + q)^2, \tag{3.24}$$

$$t = (p - \bar{p})^2, \tag{3.25}$$

$$u = (p - \bar{q})^2. \tag{3.26}$$

It remains to find some practical way to calculate the G_i in equ. (3.13) from the tree level amplitude (3.10). Progress is made by the definitions

$$v_{p,\bar{p},w}^\mu = \varepsilon^{\mu\nu\rho\sigma} p_\nu \bar{p}_\rho w_\sigma, \tag{3.27}$$

$$p_\perp^\mu = p^\mu - \frac{(p \cdot \bar{p})}{\bar{p}^2} \bar{p}^\mu - \frac{p \cdot (w - \frac{(w \cdot \bar{p})}{\bar{p}^2} \bar{p})}{(w - \frac{(w \cdot \bar{p})}{\bar{p}^2} \bar{p})^2} (w - \frac{(w \cdot \bar{p})}{\bar{p}^2} \bar{p})^\mu, \tag{3.28}$$

$$\bar{p}_\perp^\mu = \bar{p}^\mu - \frac{(\bar{p} \cdot p)}{p^2} p^\mu - \frac{\bar{p} \cdot (w - \frac{(w \cdot p)}{p^2} p)}{(w - \frac{(w \cdot p)}{p^2} p)^2} (w - \frac{(w \cdot p)}{p^2} p)^\mu, \tag{3.29}$$

$$w_\perp^\mu = w^\mu - \frac{(w \cdot \bar{p})}{\bar{p}^2} \bar{p}^\mu - \frac{w \cdot (p - \frac{(p \cdot \bar{p})}{\bar{p}^2} \bar{p})}{(p - \frac{(p \cdot \bar{p})}{\bar{p}^2} \bar{p})^2} (p - \frac{(p \cdot \bar{p})}{\bar{p}^2} \bar{p})^\mu. \tag{3.30}$$

These are constructed in such a way that p_\perp^μ is orthogonal to \bar{p}^μ and w_\perp^μ is orthogonal to p^μ and \bar{p}^μ and finally \bar{p}_\perp^μ is orthogonal to p^μ and w^μ . $v_{p,\bar{p},w}^\mu$ is perpendicular to all three vectors. With these definitions it is straightforward to read off the G_i from equ. (3.13),

$$G_1 = \frac{v_{p,\bar{p},w}^\mu T_{\mu\nu} v_{p,\bar{p},w}^\nu}{v_{p,\bar{p},w}^2}, \tag{3.31}$$

$$G_2 = (T_{\mu\nu} - G_1 g_{\mu\nu}) \frac{w_\perp^\mu w_\perp^\nu}{(w_\perp)^4}, \tag{3.32}$$

$$G_3 = (T_{\mu\nu} - G_1 g_{\mu\nu}) \frac{w_\perp^\mu \bar{p}_\perp^\nu}{(w_\perp)^2 (\bar{p}_\perp)^2}, \tag{3.33}$$

$$G_4 = (T_{\mu\nu} - G_1 g_{\mu\nu}) \frac{p_\perp^\mu w_\perp^\nu}{(p_\perp)^2 (w_\perp)^2}, \tag{3.34}$$

$$G_5 = (T_{\mu\nu} - G_1 g_{\mu\nu}) \frac{p_\perp^\mu \bar{p}_\perp^\nu}{(p_\perp)^2 (\bar{p}_\perp)^2}. \tag{3.35}$$

The results for all diagrams contributing to the scattering kernel are listed in appendix A.

Chapter 4

Analytic structure of the potential

In previous works only the leading kinematic contribution $T_{11}^{(1+)}$ was considered. This was used in a (partial wave projected) Bethe-Salpeter equation to calculate the full scattering amplitude. In this work the formalism of [18] will be used. It rests on a dispersion relation for the complete amplitude

$$T_{ab}^{(JP)}(s) = U_{ab}^{(JP)}(s) + \int_{\text{thres}^2}^{\infty} \frac{dw}{\pi} \frac{s - \mu_M^2}{w - \mu_M^2} \frac{\Delta T_{ab}^{(JP)}(w)}{w - s - i\varepsilon}, \quad (4.1)$$

where the potential U contains all the left-hand cuts and the right-hand cuts are summed up in the integral. (J, P) denotes the angular momentum and parity. In contrast to [18] where baryons were considered, the variable of integration doesn't have the dimension of an energy but of a squared energy. Since the amplitudes are defined with respect to the transformed basis (3.20) there are no additional kinematic constraints as would be the case if for example helicity eigenstates were used.

The matching point μ_M is chosen

$$\mu_M^2 = m_{\min}^2 + M_{\min}^2, \quad (4.2)$$

where the masses on the right side correspond to the pseudoscalar and vector masses of the lightest channel. This will make the full amplitude T identical to the tree-level result at a point where the scattering amplitude can be calculated perturbatively.

When the potential U has no cuts above threshold, ΔT is given by all right-hand cuts [25]:

$$\begin{aligned} \Delta T_{ab}^{(JP)}(s) &= \frac{1}{2i} [T_{ab}^{(JP)}(s + i\varepsilon) - T_{ab}^{(JP)}(s - i\varepsilon)] \\ &= \sum_{c,d} [T_{ac}^{(JP)}(s)]^\dagger \rho_{cd}^{(JP)}(s) T_{db}^{(JP)}(s). \end{aligned}$$

For a single-channel problem, the phase space is given by

$$\rho(s) = \begin{pmatrix} \frac{1}{s} \left(\frac{3}{2} + \frac{p_{\text{cm}}^2}{2M^2} \right) & \frac{1}{s^{3/2}} \left(\frac{p_{\text{cm}}^2 \omega}{\sqrt{2} M^2} \right) \\ \frac{1}{s^{3/2}} \left(\frac{p_{\text{cm}}^2 \omega}{\sqrt{2} M^2} \right) & \frac{1}{s^2} \frac{p_{\text{cm}}^4}{M^2} \end{pmatrix}. \quad (4.3)$$

It is not diagonal because of the transformation (3.20). The rescaling of equ. (3.22) was compensated with corresponding $s^{-d_{ij}}$. For large energies the rescaled phase space will approach a finite constant, a property that is crucial for the integral the master-equ. (4.1) to be well-defined.

It turns out that to solve equ. (4.1), the potential is needed at all energies above threshold, in the case of off-diagonal matrix elements above the lower threshold. As it stands, the expression (3.10) cannot be used as input for (4.1). Considering the asymptotic behavior this is already obvious: for large energies the potential will behave like a polynomial. Such a behavior is not only physically unreasonable, it also invalidates the integration.

Progress is made by looking at the analytic structure of the potential, for example for $K\rho$ scattering. The u -channel cut starts at $\sqrt{s} = m_\rho - m_K$. A Taylor expansion at the rho meson mass will therefore only converge up to threshold, $\sqrt{s} = m_\rho + m_K$, while we need the potential above threshold. To deal with this problem a trick is used. The idea is the following: instead of expanding the function in s , the argument is substituted with a function $s(\xi)$. When the potential as function of ξ is Taylor expanded the radius of convergence will now be a circle in ξ , not in s . If that function $s(\xi)$ is chosen properly the expansion in ξ (or ξ ansion) will converge for $(m_\rho - m_K)^2 < s < \Lambda_s^2$ where Λ_s can be much larger than threshold. To be more precise a Taylor expansion leads to

$$f(s) = f(s_0) + f'(s_0) \cdot (s - s_0) + f''(s_0) \cdot \frac{(s - s_0)^2}{2!} + \dots \quad (4.4)$$

When the variable is substituted this becomes

$$\begin{aligned} f(s(\xi)) &= f(s(\xi_0)) + \left. \frac{df(s(\xi))}{d\xi} \right|_{\xi=\xi_0} \cdot (\xi - \xi_0) \\ &+ \left. \frac{d^2 f(s(\xi))}{d\xi^2} \right|_{\xi=\xi_0} \cdot \frac{(\xi - \xi_0)^2}{2!} + \dots, \end{aligned} \quad (4.5)$$

and substituting back using the chain rule the result is

$$\begin{aligned} f(s) &= f(s_0) + f'(s_0) \cdot s'(\xi_0) \cdot (\xi(s) - \xi_0) \\ &+ \left(f''(s_0) (s'(\xi_0))^2 + f'(s_0) s''(\xi_0) \right) \cdot \frac{(\xi(s) - \xi_0)^2}{2!} + \dots, \end{aligned} \quad (4.6)$$

where

$$s_0 = s(\xi_0). \quad (4.7)$$

It remains to choose the function $\xi(s)$ that will lead to a convergent expansion between the lower bound Λ_u and the upper bound Λ_s when expanded around μ_E . The function $\xi(s)$ is chosen in such a way that it will be expanded around $\xi_0 = 1/2$ with a radius of convergence of $1/2$. Explicitly we use

$$s(\xi) = \Lambda_u^2 + (\Lambda_s^2 - \Lambda_u^2) \left(\frac{1 - \sqrt{\xi}}{1 + \sqrt{\xi}} \right)^{2/n} \quad (4.8)$$

or inverted

$$\xi(s) = \left(\frac{\sqrt{\frac{x}{1+x}} - \sqrt{\frac{1}{1+x}}}{\sqrt{\frac{x}{1+x}} + \sqrt{\frac{1}{1+x}}} \right)^2, \quad (4.9)$$

with $x = \left(\frac{s - \Lambda_u^2}{\Lambda_s^2 - \Lambda_u^2} \right)^n,$

where n is determined by the condition that the expansion point gets mapped onto $1/2$ which translates to

$$\left(\frac{\mu_E^2 - \Lambda_u^2}{\Lambda_s^2 - \Lambda_u^2} \right)^n = \left(\frac{\sqrt{2} - 1}{\sqrt{2} + 1} \right)^2 = 17 - 12\sqrt{2} \quad (4.10)$$

This will deform the circle of convergence. Depending on the parameters this region of convergence can look more like a heart.

The expansion in ξ (xipansion) is unique once the lower bound Λ_u , the expansion point μ_E and the upper bound Λ_s are specified. The values used are

$$\Lambda_s = 1.7 \text{ GeV}, \quad \mu_E = \frac{1}{2}(m + M + \bar{m} + \bar{M}). \quad (4.11)$$

Λ_s is a convenient choice. It turns out that the results vary only weakly with the exact choice. The xipansion point μ_E has to be placed between the thresholds where the potential is perturbative. The lower bound is more tricky. It is necessary to find the lightest exchange particle(s) that is not taken into account explicitly. One has to respect G-parity as well.

Consider for example the process $K \rho \rightarrow \pi K^*$ in the u -channel. The vertex including the pion and the ρ -meson enforces an exchange process without strangeness. This allows for example for the exchange of the $\pi, \eta, \rho, \omega, \phi$ as well as $2\pi, \pi\rho, \pi\omega, K K^*$ and so on. The single particle exchanges are all considered explicitly in this work. Two scalar particles violate the spin/parity quantum numbers and can be excluded. The lightest exchange processes are then $\pi\rho$ and $\pi\omega$. The latter violates G-parity.

The upper branch point of this lightest exchange process not considered explicitly defines the lower bound Λ_u . If this branch point is complex, the real

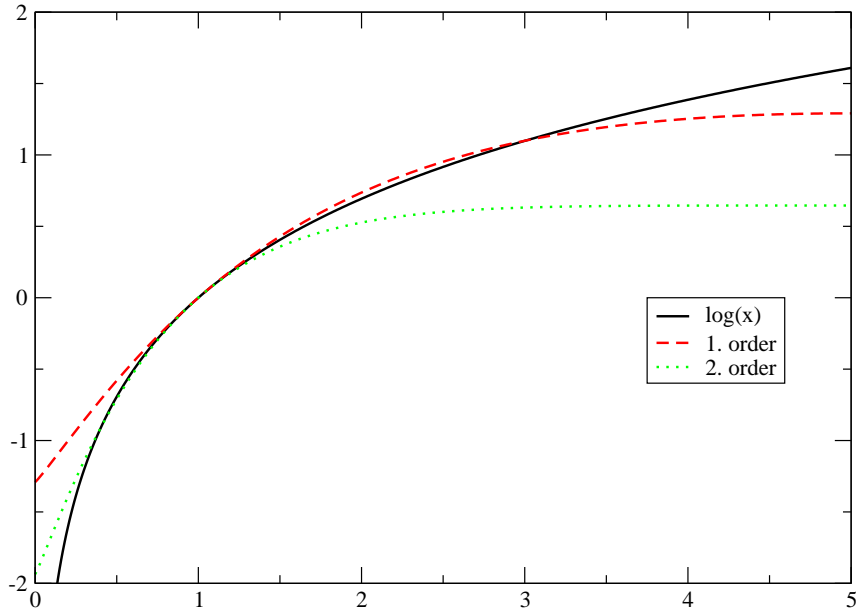


Figure 4.1: Xipansion of the function $\ln(x)$ around 1 with lower bound 0 and upper bound 5. First and second order are displayed. The zeroth order is just a constant and therefore omitted.

part is used. This defines all free parameters in the xipansion and therefore the area of convergence in the complex plane.

Here are some examples for this procedure: fig. 4.1 shows the first and second order in the xipansion of the logarithm around 1 with lower bound zero and upper bound 5. The xipansion approximates the logarithm, which corresponds to a physically reasonable high-energy behavior, well even for large energies – something a Taylor expansion would fail to achieve. The result for an upper bound of 20 is shown in fig. 4.2.

4.1 The potential from dispersion integrals

The philosophy is to evaluate all contributions from cuts inside the region where the xipansion converges exactly. Cuts outside that region will be modified by processes that are not included in our model and their contribution will therefore be xipanded.

Separating the potential into the part that is treated exactly and the rest that is xipanded requires some work. In general the potential will be of the form

$$U(s) = \alpha(s) + \frac{\beta}{s - m_s^2} + \int_{-1}^1 dx \left(\frac{\gamma(s, x)}{t(s, x) - m_t^2} + \frac{\lambda(s, x)}{u(s, x) - m_u^2} \right), \quad (4.12)$$

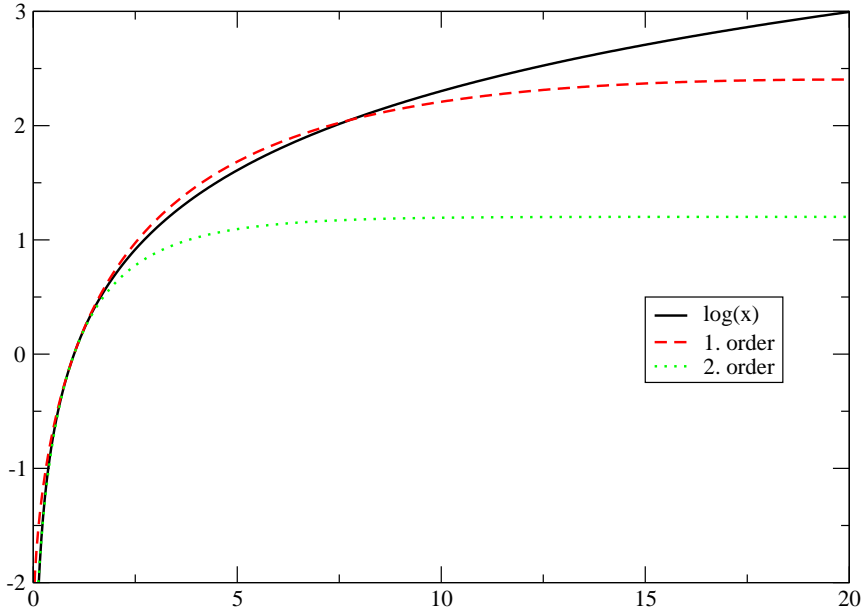


Figure 4.2: Xipansion of the function $\ln(x)$ around 1 with lower bound 0 and upper bound 20. First and second order are displayed. The zeroth order is just a constant and therefore omitted.

where the background term α contains no cuts and β is just a constant. It remains to separate the cut caused by the t - and u -channel propagator into a part that lies inside the area of convergence of the xipansion and a part outside. In the following the u -channel will be used as an example, but analogous formulas hold for the t -channel.

Progress is made by rewriting the angular integrals as dispersion integrals along the cut implied by the denominator in the equation above,

$$\int_{-1}^1 dx \frac{\lambda(s, x)}{u(s, x) - m_u^2} = \sum_{i=\pm} \int_{m_u^2}^{\infty} \frac{d\tilde{s}}{\pi} \frac{dc_i^{(u)}(\tilde{s})}{d\tilde{s}} \frac{\lambda(c_i^{(u)}(\tilde{s}), x_i^{(u)}(c_i^{(u)}(\tilde{s}))) \rho_i^{(u)}(\tilde{s})}{s - c_i^{(u)}(\tilde{s})} \quad (4.13)$$

where m_u is the mass of the exchange particle. Up to a sign the weight function ρ is given by

$$\rho_i^{(u)}(\tilde{s}) = \pm \frac{\pi}{2 p_{\text{cm}}(c_i^{(u)}(\tilde{s})) \bar{p}_{\text{cm}}(c_i^{(u)}(\tilde{s}))}. \quad (4.14)$$

The sign is a complicated function of all masses involved, explicit expressions can be found in [18].

The contour functions $c_{\pm}^{(u)}(s)$ run along the cut. They solve the equation

$$u(c_{\pm}^{(u)}(s), \pm 1) = s, \quad (4.15)$$

where $u(s, x)$ is the usual Mandelstam variable. Therefore the contour functions give the endpoints of the cut produced by an exchange particle of

squared mass s . In more detail they are

$$c_{\pm,ij}^{(u)}(\tilde{s}) = \frac{1}{2} \left(m_i^2 + M_i^2 + m_j^2 + M_j^2 - \tilde{s} \right) + \frac{(M_i^2 - m_j^2)(M_j^2 - m_i^2)}{2\tilde{s}} \\ \pm \frac{\tilde{s}}{2} \sqrt{\left(1 - 2 \frac{M_i^2 + m_j^2}{\tilde{s}} + \frac{(M_i^2 - m_j^2)^2}{\tilde{s}^2} \right) \left(1 - 2 \frac{m_i^2 + M_j^2}{\tilde{s}} + \frac{(m_i^2 - M_j^2)^2}{\tilde{s}^2} \right)} \quad (4.16)$$

where i and j are coupled-channel indices. This differs slightly from the notation of [18] where the contour function was the square root of the above expression. At the energy $c_{\pm}^{(u)}(\tilde{s})$ the angular integration on the left-hand side of (4.13) has its pole at $x_{\pm}^{(u)}(\tilde{s})$. This defines the angle implicitly. An explicit calculation results in

$$x_{\pm,ij}^{(u)}(s) = \frac{M_i^2 + m_j^2 - m_u^2 - 2 E_i(s) \omega_j(s)}{2 p_{\text{cm},i}(s) p_{\text{cm},j}(s)}, \quad (4.17)$$

with

$$E_i(s) = \frac{s - m_i^2 + M_i^2}{2\sqrt{s}}. \quad (4.18)$$

Simpler parts of the contour can be integrated directly in $\hat{s}_i = c_i^{(u)}(m)$. This substitution in (4.13) leads to

$$\sum_{i=\pm} \int_{m_1^2}^{m_2^2} \frac{d\tilde{s}}{\pi} \frac{dc_i^{(u)}(\tilde{s})}{d\tilde{s}} \frac{\lambda(c_i^{(u)}(\tilde{s}), x_i^{(u)}(c_i^{(u)}(\tilde{s})))}{s - c_i^{(u)}(\tilde{s})} \rho_i^{(u)}(\tilde{s}) \\ = \sum_{i=\pm} \int_{c_i^{(u)}(m_1^2)}^{c_i^{(u)}(m_2^2)} \frac{d\hat{s}_i}{\pi} \frac{\lambda(\hat{s}_i, x_i^{(u)}(\hat{s}_i))}{s - \hat{s}_i} \hat{\rho}_i^{(u)}(\hat{s}), \quad (4.19)$$

with

$$\hat{\rho}_i^{(u)}(\hat{s}) = \pm \frac{\pi}{2 p_{\text{cm}}(\hat{s}) \bar{p}_{\text{cm}}(\hat{s})}. \quad (4.20)$$

An explicit evaluation of the right-hand side of (4.13) over the entire range of integration can be tricky. When $c_{\pm}^{(u)}(\tilde{s})$ corresponds to one of the two thresholds involved, the integral diverges due to the center of mass momenta in equ. (4.14) and possibly additional factors of $x = \cos(\Theta)$ in $\lambda(s, x)$. In these cases the contour in (4.13) is deformed away from the real axis into a small semi-circle around that critical point. The radius of that circle has to be chosen small enough to avoid the closest sign changes in (4.14). If there is such a sign change at the critical point, a phase has to be introduced at which the integration along the semicircle around that critical point changes sign.

This entire procedure was checked by comparing both sides of equation (4.13)

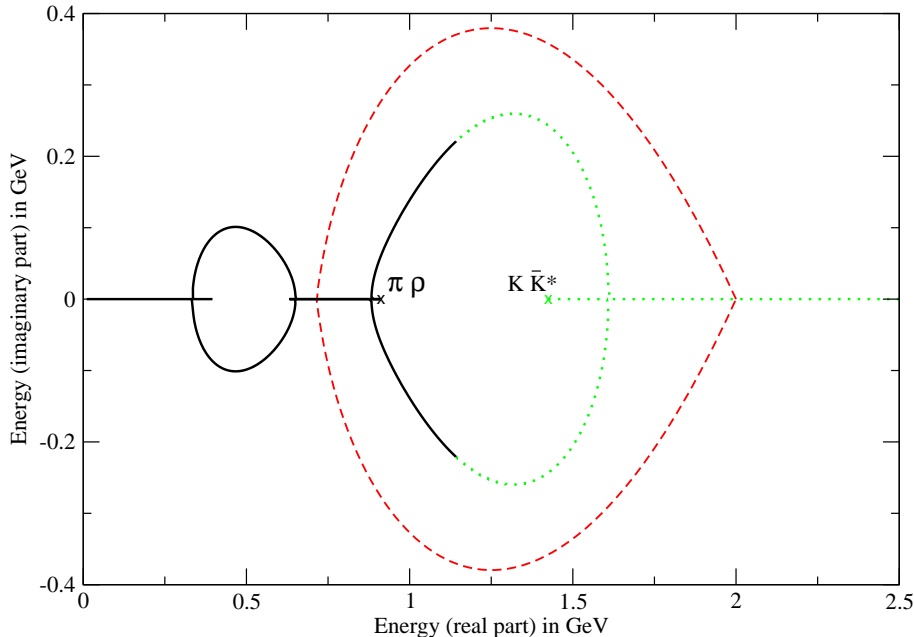


Figure 4.3: U-channel contours in the complex plane for $\pi \rho \rightarrow K \bar{K}^*$ and $\Lambda_s = 2 \text{ GeV}$. The dashed line defines the area where the xipansion converges for $\Lambda_s = 2 \text{ GeV}$. The dotted line becomes solid at the kaon mass. The two thresholds are indicated by an x .

explicitly for the masses of interest. Some cases require additional care. These will be discussed later.

The next step is to calculate the values of \tilde{s} for which the functions $c_i(\tilde{s})$ cross the border of the area of convergence of the xipansion. With these boundaries, the dispersion integral (4.13) can be separated into a part inside and outside that area, as desired.

4.1.1 Example: the exchange of a kaon in $\pi \rho \rightarrow K \bar{K}^*$

To illustrate this procedure, an example will be given: the pseudoscalar u -channel exchange of a kaon in the process $\pi \rho \rightarrow K \bar{K}^*$ where the total isospin of the incoming and outgoing state is zero. The amplitude T_{11}^{1+} as defined in equ. (3.23) is considered with the invariant amplitudes G_i taken from the appendix. Fig. 4.3 shows the position of the cuts in the complex plane. Note that the axis show the the square root of s . The radius of convergence for the xipansion is given by the dashed line. The other two lines are the cut-functions in the complex plane. The positive contour $c_+^{(u)}(\tilde{s})$ starts at high energies for small \tilde{s} and approaches points where it becomes imaginary from the right. The negative contour starts at some finite value and approaches these points from the left. The integration starts at the kaon mass, the point where the dotted line becomes solid. It ends at the point where the contour

hits the dashed line, the radius of convergence for the expansion¹.

As explained before, only cuts inside that region will be integrated. In this example the positive cut consists of three intervals:

interval	start[GeV ²]	stop[GeV ²]	sign	
1	0.246	0.571	+1), (4.21)
2	0.571	0.609	+1	
3	0.609	0.860	-1	

the last number gives the sign in equ. (4.14). The first interval starts at the squared exchange mass, the kaon mass. At $(m_{K^*} - m_\pi)^2 = 0.571 \text{ GeV}^2$ the contour hits the real axis and moves to the right. It changes direction at threshold which is reached at $(m_\pi m_K^2 + m_\rho m_{K^*}^2)/(m_\pi + m_\rho) - (m_\pi m_\rho) = 0.609 \text{ GeV}^2$. For values larger than 0.86 GeV^2 the contour lies outside the domain where it has to be expanded.

Integrating the first interval as detailed in equ. (4.13) doesn't cause any problems, but at the point where the contour reaches the lower threshold, the product of the incoming and outgoing center of mass momenta vanishes, resulting in a divergence in equ. (4.14, 4.17). As mentioned before, this problem can be tackled by deforming the integration contour in (4.13) into the complex plane so that it goes around the dangerous point at some radius ε . In equ. (4.14) the sign changes at that critical point. It remains to generalize the sign change that it can also be used for complex \tilde{s} . Fig. 4.4 shows the function that has to be integrated on a semicircle with radius $\varepsilon = 0.01 \text{ GeV}^2$ and for the larger radius $\varepsilon = 0.05 \text{ GeV}^2$ when the sign change is ignored. From this figure it is obvious in both cases where the sign-change has to be placed. The discontinuity can be traced back to the square root in the expression for the center of mass momentum. It occurs where the imaginary part of the argument changes sign. This information allows to implement the sign change at the correct phase. The phase also depends on the radius of the semicircle in the complex plane as can be seen from the two examples given. The situation is displayed schematically in fig. 4.5 where the dashed line separates the regions with different sign. The smaller the radius is chosen the closer the phase will be to $\pi/2$. In practice the radius should not be too small to avoid numerical difficulties but it has to be small enough to avoid other sign changes close to the critical point in question. Values in between the two examples given above turn out reasonable.

The difference between this result and the exact integration will be expanded and added. For the current example the details are shown in fig. 4.6 where the exact potential and the dispersive integral are displayed together with the final result for the integration. The difference between the former two is displayed in fig. 4.7. It has to be expanded and added to the dispersive integral to get the final potential. The result of the expansion is also shown in that figure.

¹If the exchange particle were a K^* instead of a K , the contour would be of the same form with the only difference that the dotted line would turn solid further to the left.

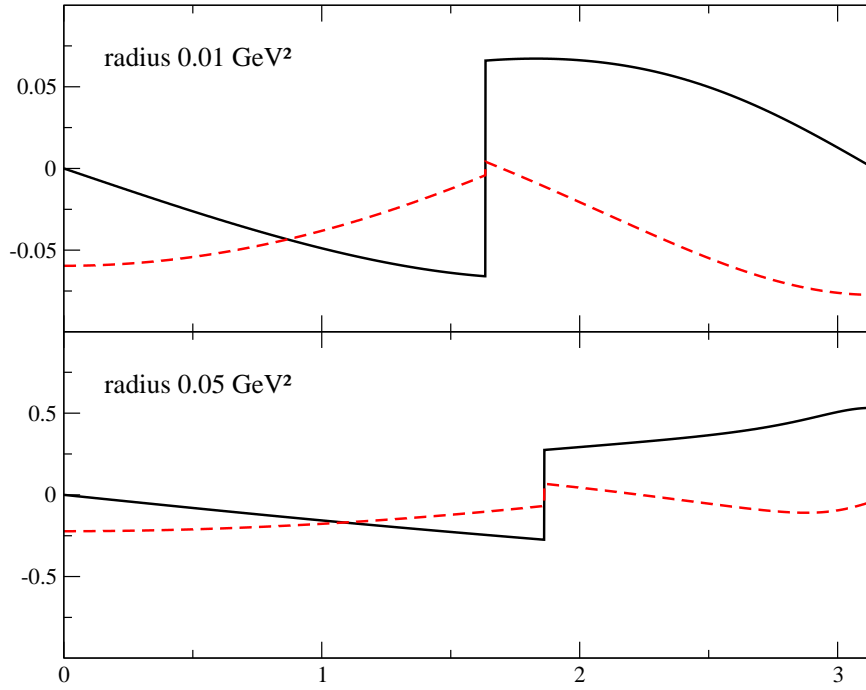


Figure 4.4: Real and imaginary part of the integrand in equ. (4.13) along a small semicircle in the complex plane around the lower threshold. The upper plot corresponds to the radius $\varepsilon = 0.01 \text{ GeV}^2$, the lower plot to $\varepsilon = 0.05 \text{ GeV}^2$. The solid lines show the real part, dashed curves correspond to the imaginary part.

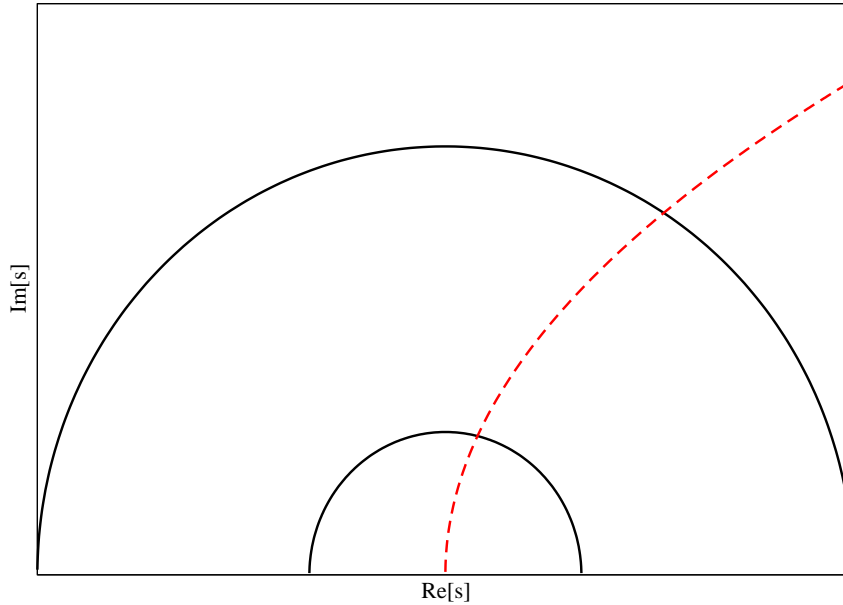


Figure 4.5: Position of the sign change schematically. The solid lines show the path of integration in the complex plane around the critical point. The dashed line separates the regions where with different sign in equ. (4.14).

As one can see, for not so high energies the result of the dispersive integral agrees well with the exact expression even so only a small part of the cut is integrated. This results in a small function to be expanded. This expansion also agrees well up to about 2 GeV, but the asymptotic behavior is modified.

4.2 Perturbative analysis of the scattering amplitude

Beside poles in the region of integration, other issues may arise when the partial wave projected amplitudes (3.23) are evaluated either by an angular or by a dispersive integration. These issues will be presented in this section together with possible solutions.

To see that the solutions are indeed correct, a check is needed. This is provided by a perturbative analysis of the master-equation (4.1) when it is iterated once with $T_0(s) = U(S)$, where spin, parity and coupled-channel indices have been suppressed. Let the potential U be the sum of the problematic diagram in question and some simple contact term without derivatives. The nominator will be of the form $(U \cdot \rho \cdot U)$ and contain two mixed terms which can be interpreted as triangle diagrams. Let the problematic diagram be for instance a u -channel exchange process between scalar particles. The

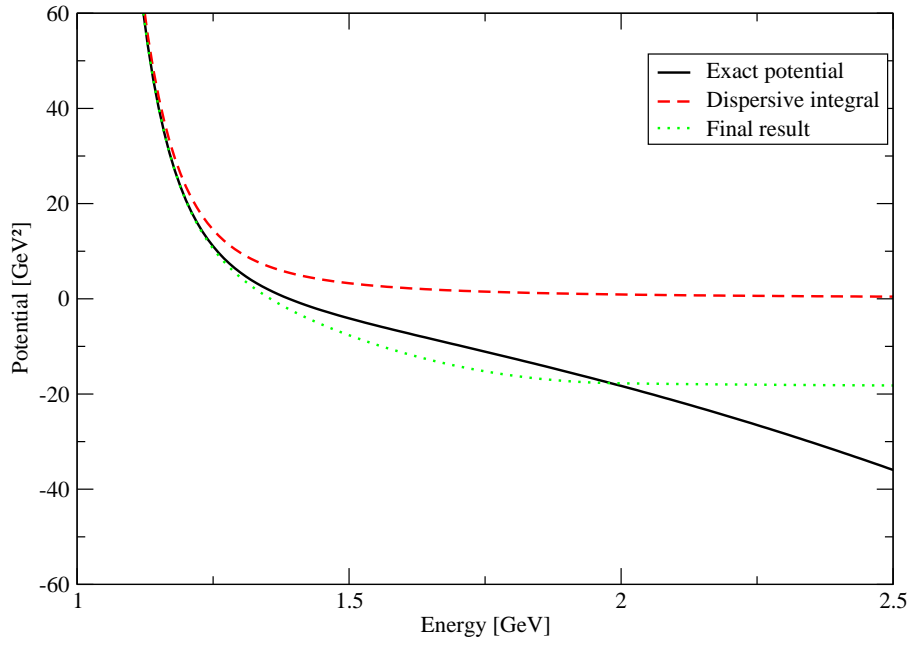


Figure 4.6: Results of the exact and dispersive integration in the case $\pi \rho \rightarrow K$

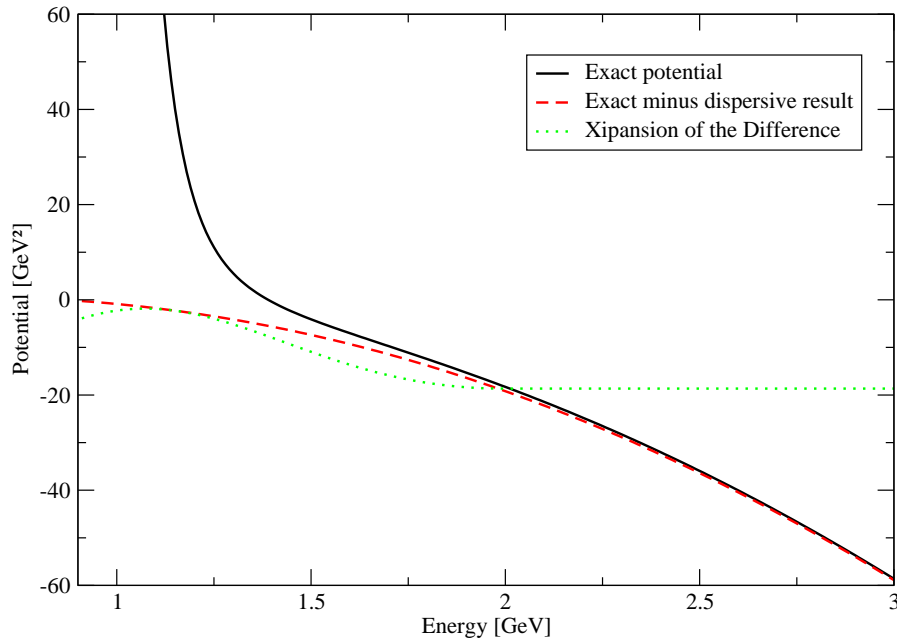


Figure 4.7: This plot shows the exact potential in the case $\pi \rho \rightarrow K \bar{K}^*$ together with the difference between the former and the dispersive integration. The xipansion of this difference is also displayed.

equation above gives

$$\begin{aligned} T_{\Delta}(s) &= \int_{\text{thres}^2}^{\infty} \frac{dw}{\pi} (1 \cdot \rho(w) \cdot U_u(w)) \frac{1}{w - s - i\varepsilon}, \\ U_u(w) &= \int_{-1}^1 \frac{dx}{u(w, x) - m^2}, \end{aligned} \quad (4.22)$$

where the subtraction at μ_M^2 and coupling constants have been ignored. Alternatively this diagram can be calculated unambiguously by the use of Feynman parameters resulting in

$$\begin{aligned} T_{\Delta}(s) &= \int \frac{d^4l}{(2\pi)^4} \frac{-i}{(l^2 - \bar{m}^2)((l - \bar{q})^2 - m_u^2)((w - l)^2 - \bar{M}^2)} \\ &= \frac{-1}{16\pi^2} \int_0^1 dz_3 \int_0^{1-z_3} dz_2 \frac{1}{D}, \\ D &= (M^2 - s)z_2 + s z_2^2 + m^2(1 - z_2 - z_3) + (m_u^2 - \bar{M}^2)z_3 \\ &\quad + (\bar{M}^2 - \bar{m}^2 + s)z_2 z_3 + \bar{M}^2 z_3^2 - i\varepsilon. \end{aligned} \quad (4.23)$$

When both ways to calculate the triangle diagram agree, the prescription to calculate the potential $U_u(s)$ is correct.

4.2.1 Anomalous thresholds

The angular integration leads to logarithms which will give incorrect results if calculated on the first Riemann sheet. For a simple example consider a u -channel exchange process where all particles are scalars.

The integral

$$\int_{-1}^1 \frac{dx}{u(s, x) - m^2} \quad (4.24)$$

is of the form

$$\int_{-1}^1 \frac{dx}{A(s) + x B(s)} = \frac{1}{B(s)} \ln \left(\frac{A(s) + B(s)}{A(s) - B(s)} \right), \quad (4.25)$$

where the right-hand side is the result of a formal integration. $B(s)$ is a multiple of the product of the incoming and outgoing center of mass momentum – and therefore complex between thresholds. If $A(s)$ changes sign in that region, one has to be careful to evaluate the logarithm on the correct Riemann sheet. Naive evaluation of the integral together with a correction

$$- \frac{2\pi i}{B(s)} \Theta(\Im[A(s) B(s)]) \quad (4.26)$$

will lead to a result that is continuous where $A(s)$ changes sign. A nominator of the form x^n would otherwise lead to a discontinuity in the n -th derivative

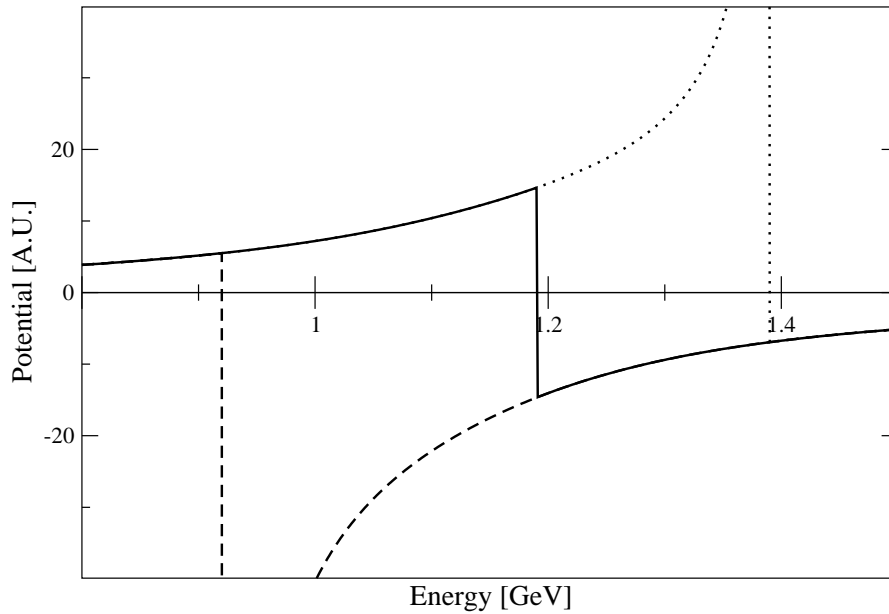


Figure 4.8: This plot shows the result of the angular integration of a u -channel propagator when a kaon is exchanged in $\pi \rho \rightarrow K K^*$. A naive integration leads to the solid line. The discontinuity can be cured in two ways, see text for further explanation.

of the resulting function of s .

An example is shown in fig. 4.8. The process considered is $\pi \rho \rightarrow K K^*$ with the exchange of a kaon in the u -channel. All particles are treated as scalars. The solid line is the result of a naive integration of equ. (4.24). The discontinuity is at 1.190 GeV. In principle this discontinuity can be cured in both directions, either as in equ. (4.26) or with the negative of this correction and the sign of the argument of the Theta-function reversed. The prescription given in the equation above will lead to the continuation indicated by the dashed line while the reversal of signs in the prescription leads to the dotted continuation. The dashed curve ends at the $\pi \rho$ threshold while the dotted curve is discontinuous at the $K K^*$ threshold.

The potential will be needed above the lower threshold and has to be continuous. Therefore the prescription that leads to the dashed line is employed.

The physical situation is shown in fig. 4.9 for $\pi \rho \rightarrow K K^*$ with a pseudoscalar meson in the u -channel for the amplitudes $T_{11}^{(1+)}$ and $T_{12}^{(1+)}$ as defined in equ. (3.23). The dashed line indicates the result of a naive integration while the solid line shows the effect of the correction. Note that the correction diverges at thresholds. This is only a square root singularity in Mandelstam s and can therefore still be integrated. The correctness of this prescription can be checked as explained before by inserting the result into the iterated master-equation (4.22) and comparing to the Feynman parameterization (4.23).

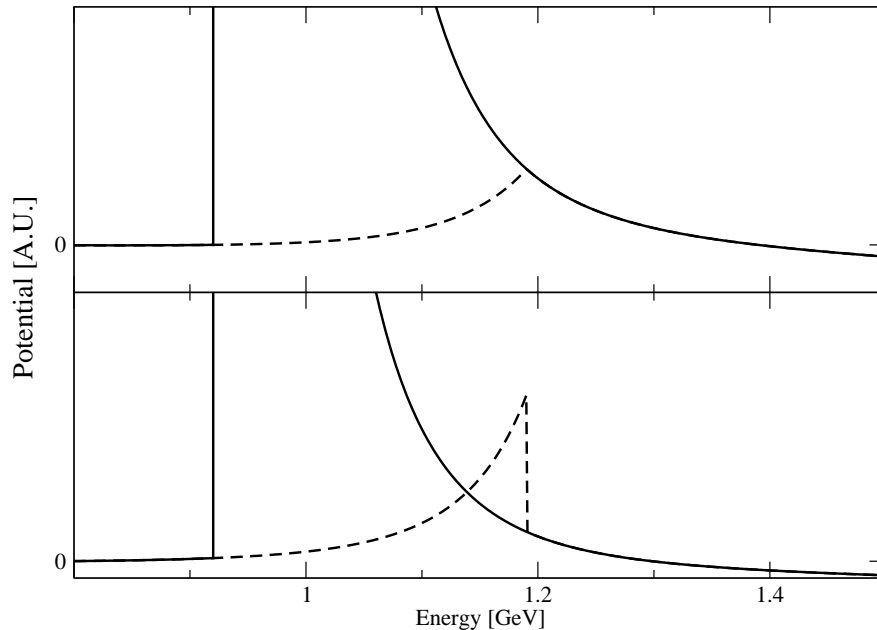


Figure 4.9: This plot shows the potential $T_{11}^{(1+)}$ and $T_{12}^{(1+)}$ for a kaon exchange in the u -channel in $\pi \rho \rightarrow K K^*$. See text for further explanation.

4.2.2 Cuts on the real axis: $\pi \rho \rightarrow \pi \rho$

In some cases additional complications arise from the exchange of Goldstone bosons in the u -channel. Consider the exchange of a u -channel pion in the process $\pi \rho \rightarrow \pi \rho$. ρ -mesons are unstable and can decay into two pions. This allows the propagating particle in the u -channel to be on-shell, resulting in a pole in the angular integration for $1.11 \text{ GeV} < \sqrt{s} < 4.26 \text{ GeV}$. In the angular integration this pole can be treated by naively integrating

$$\int_{-1}^1 dx \frac{1}{A(s) + x B(s)} = \frac{1}{B(s)} \ln(A(s) + x B(s)) \Big|_{x=-1}^{x=+1}. \quad (4.27)$$

Fig. 4.10 shows the real and imaginary part of the result of the angular integral in equ. (4.27). The phase space function needed in equ. (4.22) is simply

$$\rho(w) = \frac{p_{cm}(w)}{8 \pi \sqrt{s}}. \quad (4.28)$$

A numerical comparison with the result of the Feynman parameterization shows that this prescription indeed works. The two functions have to be compared slightly above the real axis when there is a cut present.

This cut will also show up when the angular integral is rewritten as a dispersive integral. It can be treated by subtracting it from the integrand and

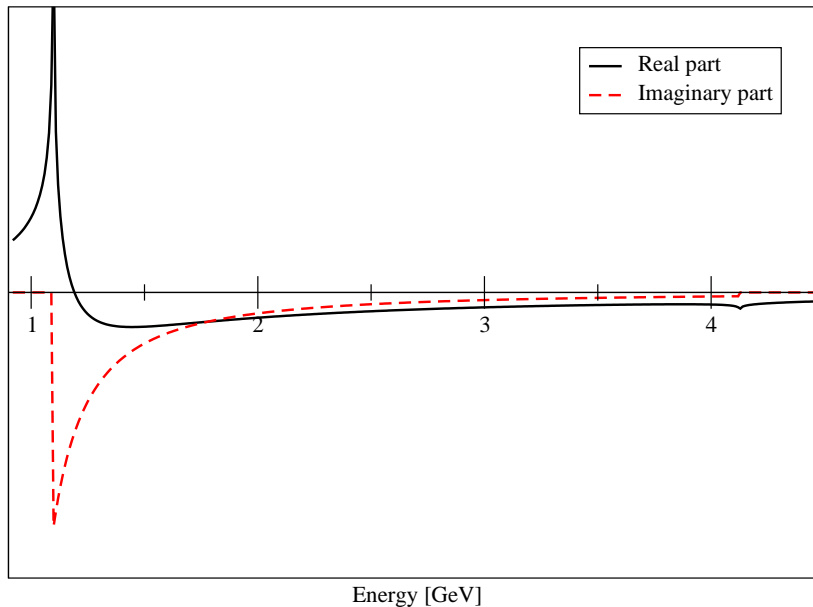


Figure 4.10: Real and imaginary part of the result of the angular integral in equ. (??) for the case $\pi\rho \rightarrow \pi\rho$.

adding 2π times the residue. This leads to the same result when the dispersive integral goes to infinity, but it takes a lot more CPU-time. In practice the calculation is therefore done in another way. The potential is divided into two parts, \bar{U} and \tilde{U} . The latter contains the contribution from the cut on the real axis. Fig. 4.11 shows the contours schematically in that case. The positive contour starts at the right end of the cut and goes down along the real axis until it becomes complex; the negative contour starts at the other end of the cut and goes to lower energies until it turns around at threshold and leaves the real axis at the same point as the positive contour, but into the opposite direction.

One possibility to calculate the contribution from the cut, \tilde{U} , would be to perform the dispersive integral only on the positive cut and only up to the point where the negative cut starts. As mentioned before, this would be very CPU-intensive. Instead one can use the angular integration to calculate the imaginary part along the cut. From this imaginary part one can calculate the real part using a dispersion integral. It remains to calculate the rest of the potential, \bar{U} . Starting the dispersive integration at the left end of the cut would be numerically difficult because the potential diverges at that point. Since the imaginary part has to be zero at that place we can use the information that both contours have to cancel identically and start the integration anywhere between the lower end of the cut on the real axis and the point where the contours leave into the complex plane. This requires to start the integration in equ. (4.13) at different squared masses for the positive and negative contours and will then allow to calculate \bar{U} as described before.

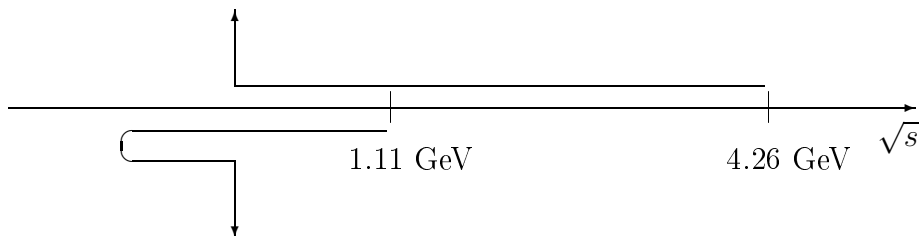


Figure 4.11: Position of the contours in $\pi \rho \rightarrow \pi \rho$ schematically. The positive cut is drawn above the real axis, the negative cut below the real axis.

4.2.3 Cuts on the real axis: $\pi \phi \rightarrow \bar{K} K^*$

Figure 4.12 shows the position of the cuts schematically for the u -channel exchange of a kaon in the process $\pi \phi \rightarrow \bar{K} K^*$ where the final state is the combination with positive G-parity. The cut on the real axis starts at 1.39 GeV and ends at 1.56 GeV. In contrast to the previous example it is partly realized by the negative contour and partly by the positive contour.

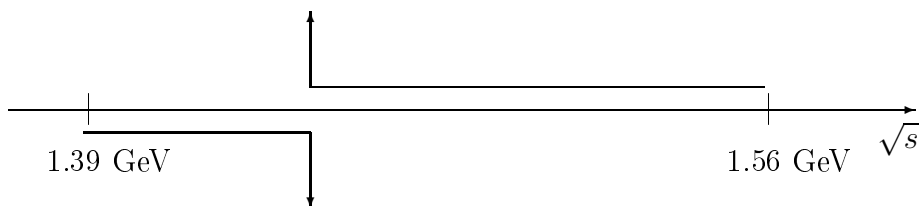


Figure 4.12: Position of the contours in $\pi \phi \rightarrow K K^*$ schematically. The positive cut is drawn above the real axis, the negative cut below the real axis.

The integration along the cuts can be treated as before. On the negative contour one has to interpret the contour as below the real axis. The path of integration can be deformed by adding a closed contour which encases no poles. Figure 4.13 shows one possible way to do so. Without modifications the negative contour corresponds to the black solid line and the dashed red line. The additional closed contour is given by the solid black line and the green dashed line. Effectively it is enough to integrate along the dashed and the dotted path.

4.2.4 Cuts on the real axis: $\pi K^* \rightarrow K \rho$

The u -channel exchange of a pion in the transition $\pi K^* \rightarrow K \rho$ is displayed in fig. 4.14. This example is similar to the previous one with the exception

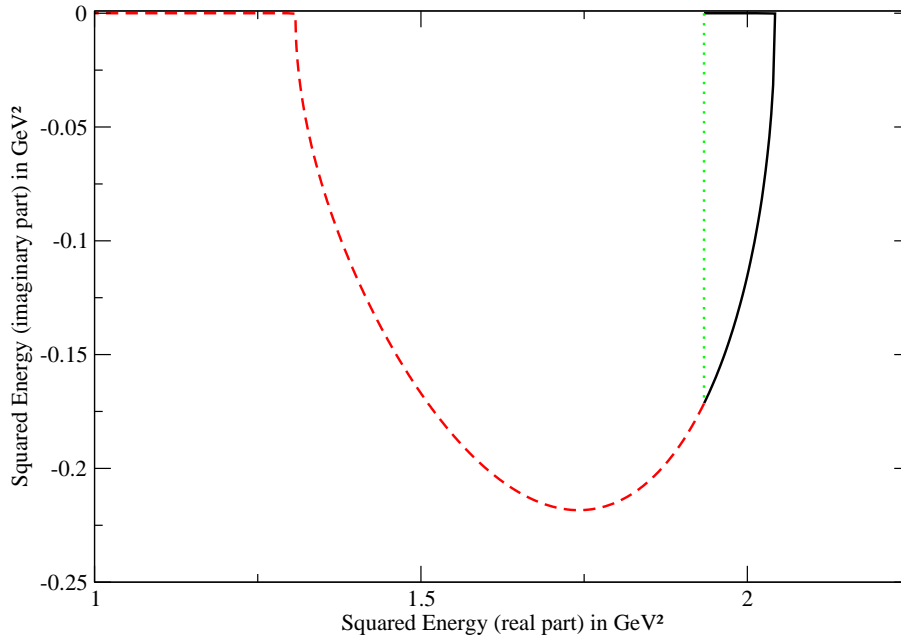


Figure 4.13: One possible deformation of the integration contour in the reaction $\pi\phi \rightarrow \bar{K}K^*$ with a kaon in the u -channel. Note that the axis show Mandelstam s and not the energy.

that the negative contour first decreases until it reaches threshold where it turns around and moves towards higher energies until it leaves the real axis. In the region between 1.26 GeV and 1.27 GeV the two contributions from the negative contour cancel each other. The cut on the real axis starts at 1.27 GeV and the starting point of the positive contour.

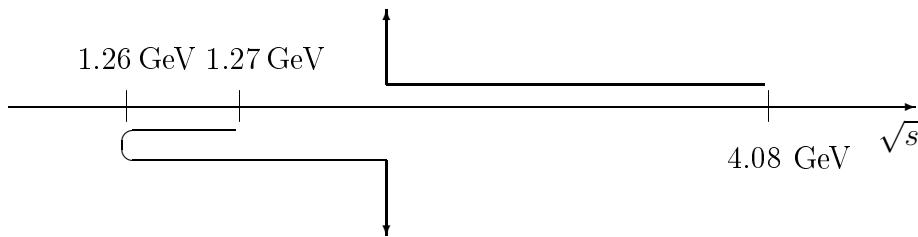


Figure 4.14: Position of the contours in $\pi K^* \rightarrow K\rho$ schematically. The positive cut is drawn above the real axis, the negative cut below the real axis.

Chapter 5

Computation of the scattering amplitude

In this section the methods to solve equation (4.1),

$$T_{ab}^{(JP)}(s) = U_{ab}^{(JP)}(s) + \int_{\text{thres}^2}^{\infty} \frac{dw}{\pi} \frac{s - \mu_M^2}{w - \mu_M^2} \frac{\Delta T_{ab}^{(JP)}(w)}{w - s - i\varepsilon}, \quad (5.1)$$

with

$$\Delta T_{ab}(s) = \sum_{c,d} T_{ac}^-(s) \rho_{cd}(s) T_{db}^+(s), \quad (5.2)$$

will be presented. In the equation above the upper indices + and - note the evaluation slightly above and below the real axis, respectively. Coupled-channel and Lorentz indices have been suppressed. The discussion will summarize the results of [18], similar problems were discussed in [26, 27, 28].

5.1 Case 1: real potential

In a first step it will be assumed that the potential has no imaginary part. As shown in [18], an important first step is the solution of the integral equation

$$\begin{aligned} \varsigma(s) = & -\bar{U}(s) \rho(s) \\ & - \int_{\text{thres}^2}^{\infty} \frac{dw}{\pi} \frac{s - \mu_M^2}{w - \mu_M^2} \frac{\varsigma(w) (U(s) - U(w)) \rho(s)}{w - s} \end{aligned} \quad (5.3)$$

for ς . Equation (5.3) can be solved numerically on a grid. It turns out useful to perform the calculations in the variable $1/s$ and to use Gaussian points distributed between critical points as grid. The critical points include all thresholds and the endpoints of cuts on the real axis. More details can be found in [18].

The second step is to calculate two dispersive integrals,

$$B_{ab}(s) = \int_{(m_c+M_c)^2}^{\infty} \frac{dw}{\pi} \frac{s - \mu_M^2}{w - \mu_M^2} \frac{\varsigma_{ac}(w) U_{cb}(w)}{w - s}, \quad (5.4)$$

$$D_{ab}(s) = \delta_{ab} + \int_{(m_b+M_b)^2}^{\infty} \frac{dw}{\pi} \frac{s - \mu_M^2}{w - \mu_M^2} \frac{\varsigma_{ab}(w)}{w - s}. \quad (5.5)$$

The solution of the master-equation (4.1) can then be written as

$$T(s) = U(s) - D^{-1}(s) \cdot B(s). \quad (5.6)$$

The dispersive integrals for B and D are performed on a grid which includes the threshold, is equidistant between thresholds and gets more coarse at higher energies. To calculate $\varsigma(s)$ on this grid equ. (5.3) is used again, this time on an asymmetric grid (for the variable w the Gaussian grid is used again, while for the variable s the new grid is employed). The right-hand side is calculated with s on the new grid and w on the Gaussian grid.

5.2 Case 2: complex potential

When the interaction has an imaginary part above threshold things get more complicated. In a first step the potential is separated into the contribution from the cut on the real axis and the rest:

$$U(s) = \bar{U}(s) - \frac{1}{2i} \int_{\text{thres}^2}^{\infty} \frac{dw}{\pi} \frac{U^{(+)}(w) - U^{(-)}(w)}{w - s}. \quad (5.7)$$

The contribution from \bar{U} can be treated as before. It is not yet clear how to treat the integral part of the equation above.

Fig. 5.1 illustrates the situation in the diagonal $\bar{K} K^*$ channel with spin and isospin zero and positive G-parity. The exact result which contributes to the potential $U(s)$ shows a strong energy dependence at the point where the cut starts. Once the integral in equ. (5.7) is subtracted the potential becomes almost linear.

The imaginary part of the exact potential for the physical case of the exchange of a pion between a K -meson and a \bar{K}^* -meson in the u -channel in the $(I^G, S) = (0^+, 0)$ sector is shown in fig. 5.2. In the left column, s-wave, the transition amplitude between s- and d-wave and d-wave are displayed.

A discontinuity in the imaginary part for d-wave scattering is expected to invalidate a treatment of the imaginary part. For example a finite jump in U would lead to a logarithmic divergence in the integral (5.4). The imaginary part is a consequence of the instability of the K^* and its possible decay into a kaon and a pion which also gives the K^* its width. Averaging the imaginary part over the spectral distribution of the incoming and outgoing vector particle will make the potential continuous again. A spectral distribution $\rho_S(s)$

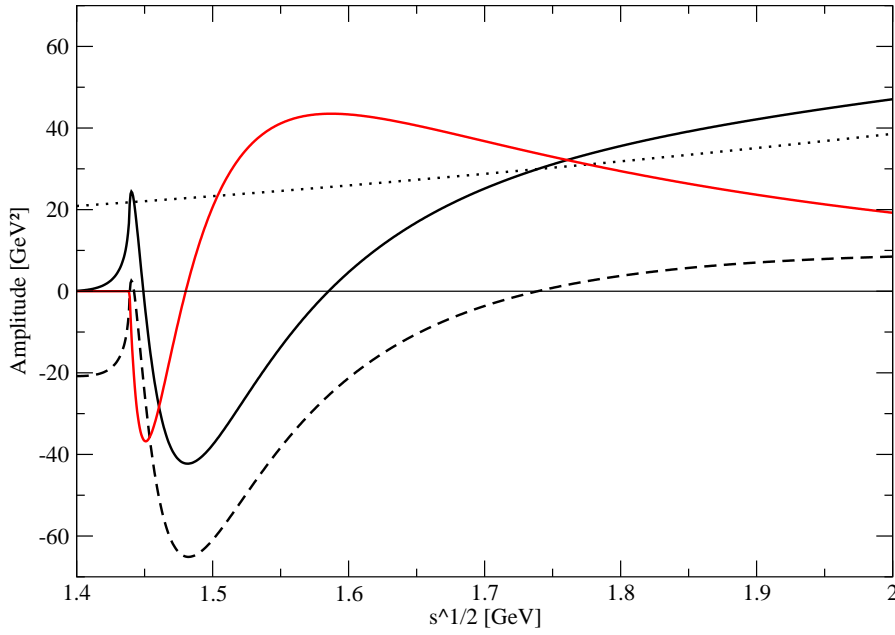


Figure 5.1: This figure shows the real part of the exact potential (solid black line), the imaginary part of the exact potential (solid red line), the real part of the integral in equ. (5.7) (dashed line) and the difference of the real parts (dotted line) in the case $\bar{K} K^* \rightarrow \bar{K} K^*$ with a pion in the u -channel.

can be found in [29]. In the process of averaging another problem arises: the integral

$$\int_{(m_K+m_\pi)^2}^{\infty} dm_1^2 \int_{(m_K+m_\pi)^2}^{\infty} dm_2^2 \rho_S(m_1^2) \rho_S(m_2^2) U(s, m_1^2, m_2^2)$$

includes a combination of K^* masses for which the cut starts at threshold:

$$\begin{aligned} m_\pi + m_1 &= s, \\ c_-(s, m_\pi^2, m_2^2) &= s, \end{aligned}$$

where c_- is the contour function. At this point (and the point with m_1 and m_2 interchanged) in the integration, negative powers of the center of mass momentum will diverge. These divergences are integrable if the s-wave is involved. For the d-wave it is necessary to deform the contour of both integrations in the averaging slightly away from the real axis. To do so the expression for the spectral distribution has to be replaced by some analytic function which coincides with the non-analytic formula in [29] on the real axis. Explicitly, the formula used is

$$\begin{aligned} \lambda(s) &= (s - (m_\pi + m_K)^2) \cdot (s - (m_\pi - m_K)^2), \\ f_R(s) &= \frac{1}{16\pi^2} \left(\frac{\sqrt{\lambda(s)}}{2s} (\ln(-m_\pi^2 - m_K^2 + s - \sqrt{\lambda(s)}) \right) \end{aligned}$$

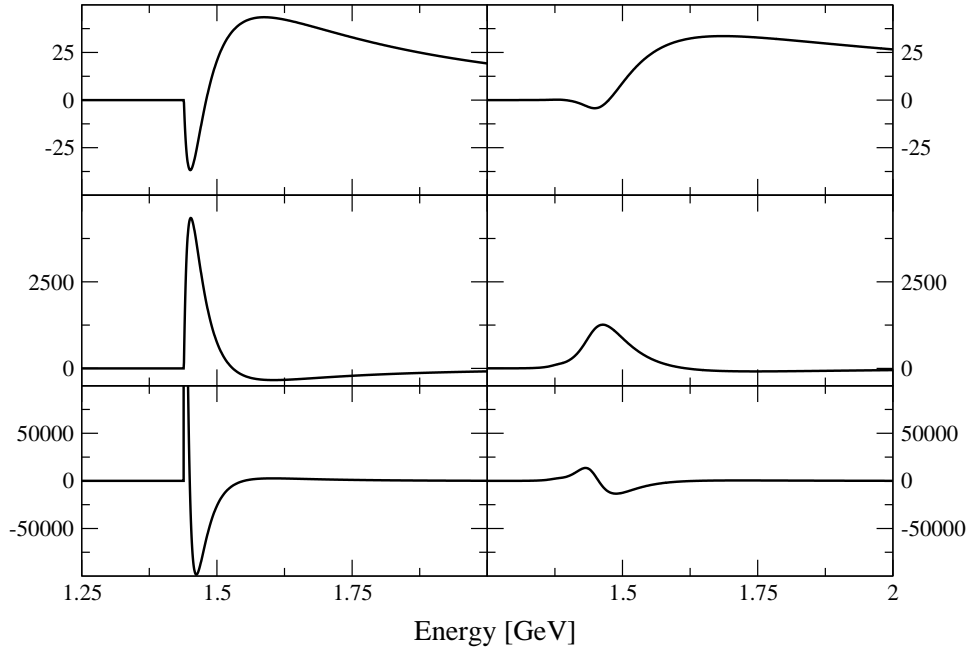


Figure 5.2: This figure shows the imaginary part of the potential in the case $\bar{K} K^* \rightarrow \bar{K} K^*$ with a pion in the u -channel. On the right side the potential was averaged over the spectral distribution of the incoming and outgoing K^* . The first row corresponds to $T_{11}^{(1+)}$, the second row shows $T_{12}^{(1+)} = T_{21}^{(1+)}$ and the last row $T_{22}^{(1+)}$.

$$\begin{aligned}
& -\ln(-m_\pi^2 - m_K^2 + s + \sqrt{\lambda(s)}) + 2), \\
f_I(s) &= \frac{i\sqrt{\lambda(s)}}{16\pi s}, \\
g_R(s) &= (s - (m_\pi + m_K)^2) \cdot (f_R(s) - f_R(m_{K^*}^2)), \\
g_I(s) &= (s - (m_\pi + m_K)^2) \cdot f_I(s), \\
\rho_{K^*} &= -i g_\rho \frac{N}{s} \frac{g_I(s)}{(|g_I(m_{K^*}^2)|)} \\
& \cdot \frac{1}{(s - m_{K^*}^2 + m_{K^*} g_\rho (g_R(s) + g_I(s)) / (|g_I(m_{K^*}^2)|))} \\
& \cdot \frac{1}{(s - m_{K^*}^2 + m_{K^*} g_\rho (g_R(s) - g_I(s)) / (|g_I(m_{K^*}^2)|))}, \quad (5.8)
\end{aligned}$$

with $g_\rho = 0.051$ GeV and N a constant to normalize the integral over this expression to unity. Compared to the expression give in [29], the formula above contains an additional factor $1/s$ which makes the spectral function normalizable and thus allows to drop the cutoff used in the original work.

The result of the imaginary part of the potential with this spectral distribution is shown in the right column of fig. 5.2.

Using the spectral average also means changing the $\bar{K} K^*$ threshold to $2m_K + m_\pi$. In the region between this new threshold and the nominal threshold the potential develops additional imaginary contributions, for example from the exchange of an η in the u -channel but also from the exchange of a rho-meson. The calculations for the exchange of a pion have already proven to be tedious, averaging the exchange of a particle with width like the rho-meson is beyond the scope of this work. Therefore the pseudoscalar exchange processes will not be considered in the following.

Chapter 6

Results

In the sectors with isospin or strangeness larger than one no resonances are generated. The remaining sectors will be discussed in the following. Close to a resonance the scattering amplitude behaves like

$$T_{ab}(\sqrt{s}) = -\frac{s}{M \bar{M}} \frac{g_1 g_2 M_R}{\sqrt{s} - m_R + i \Gamma/2}. \quad (6.1)$$

In the case of bound states the width Γ vanishes. To analyze the scattering amplitude in more details the absolute value of the derivative of the scattering amplitude with respect to energy,

$$\left| \frac{dT_{ab}(\sqrt{s})}{d\sqrt{s}} \right|. \quad (6.2)$$

is used in the calculations. Close to a resonance this will be fitted to the corresponding expression obtained from equ. (6.1) to evaluate the position M_R , width Γ and coupling constants g_i of a state. In the case of a bound state the inverse is used.

6.1 Results for Weinberg-Tomozawa Interaction

In a first step the results will be discussed in the case when only the Weinberg-Tomozawa interaction is considered and the expansion is performed to first order. S- and d-wave will be considered.

6.1.1 $(I, S) = (\frac{1}{2}, 1)$

Fig. (6.1) shows the real and the imaginary part of the scattering amplitude for $(I^G, S) = (\frac{1}{2}, 1)$. The dominant effect is a narrow resonance that has a mass of 1.233 GeV and a width of 4 MeV. The coupling constants as defined

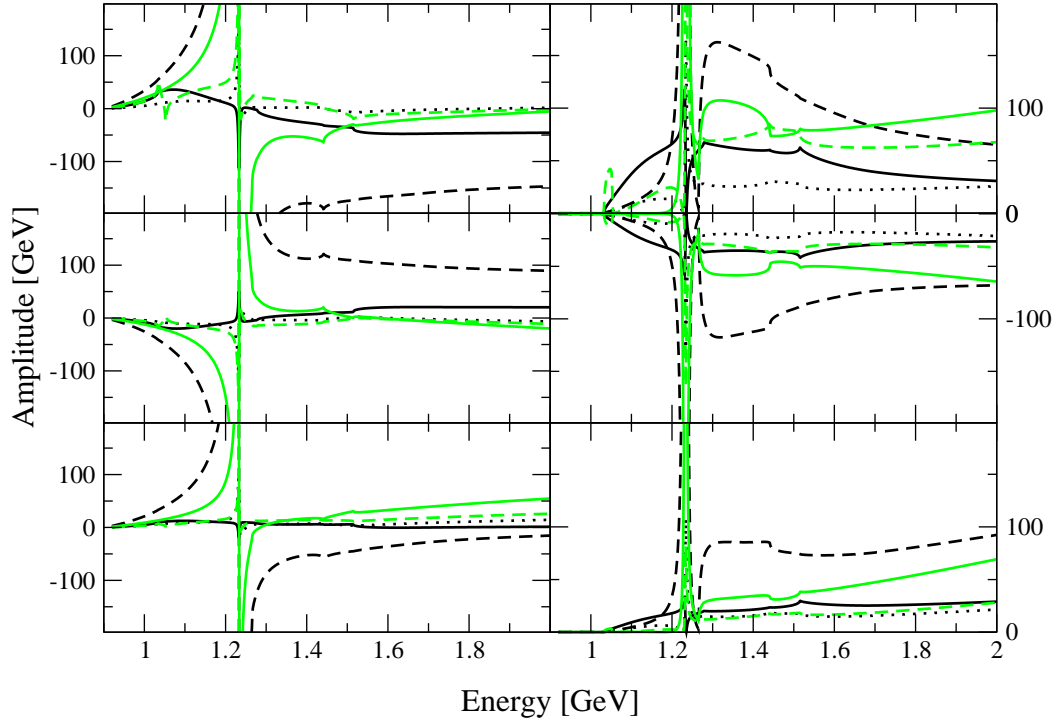


Figure 6.1: This figure shows the amplitudes for $(I^G, S) = (\frac{1}{2}, 1)$ when only the Weinberg-Tomozawa interaction is considered. The left column show the real part, the second column the imaginary part of the scattering amplitude. The first row corresponds to the s-wave, the second row to to the transition amplitude between s- and d-wave and the last row to d-wave. The solid black line corresponds to the πK channel, the dashed black line to ρK , the dotted black line to ωK , the solid green line to ηK^* and the dashed green line to ϕK .

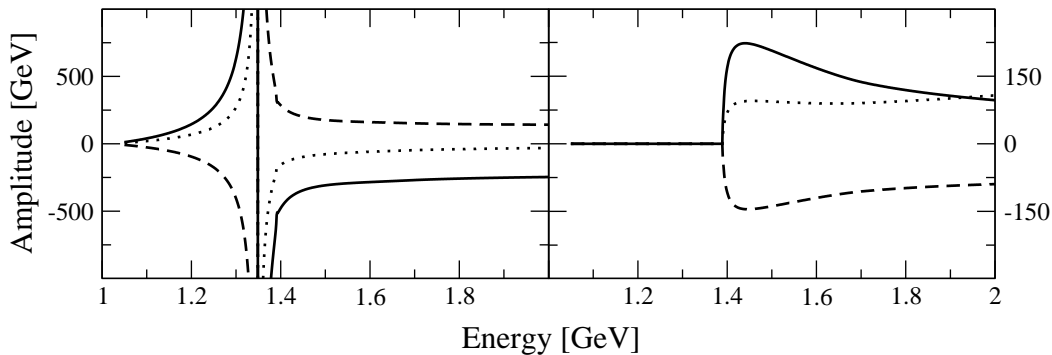


Figure 6.2: This figure shows the amplitude for $(I^G, S) = (0^+, 0)$, the $\bar{K} K^*$ channel, when only the Weinberg-Tomozawa interaction is considered. The left figure shows the real part, the right figure the imaginary part of the scattering amplitude. The solid line corresponds to the s-wave, the dashed line to the transition amplitude between s- and d-wave and the dotted line to d-wave.

in equ. (6.1) are

			wave	πK^*	ρK	ωK	ηK^*	ϕK	
mass	width		s	0.35	3.1	0.41	2.1	0.58	. (6.3)
1.233 GeV	4 MeV		$s - d$	0.22	2.4	0.34	1.4	0.37	
			d	0.14	1.8	0.27	0.88	0.24	

This resonance corresponds to the $K_1(1270)$ which has a width of 90 MeV. As in [15] the ρK and the ηK^* channels are dominant, but here the binding energy is higher. This also explains the small width: the resonance position is near the ρK and the ωK threshold. With those two channels closed, the width gets to small.

When only the s-wave is considered as in [15] the position and width turn out to be 1.216 GeV and 5 MeV respectively.

In the amplitudes that are not dominated by the $K_1(1270)$ one can also see a weak signal of the $K_1(1400)$. According to the PDG this state has a width of 174 MeV. A quantitative analysis will be avoided.

6.1.2 $(I^G, S) = (0^+, 0)$

In this one channel problem there is a bound state with a mass of 1348 MeV. The coupling constants are 3.6, 2.5 and 1.7 for s-wave, the transition between s- and d-wave and for d-wave respectively. The state corresponds to the $f_1(1285)$ which came out at a higher mass in [15]. When the d-wave is ignored, the binding is again slightly higher, leading to a mass of 1336 GeV.

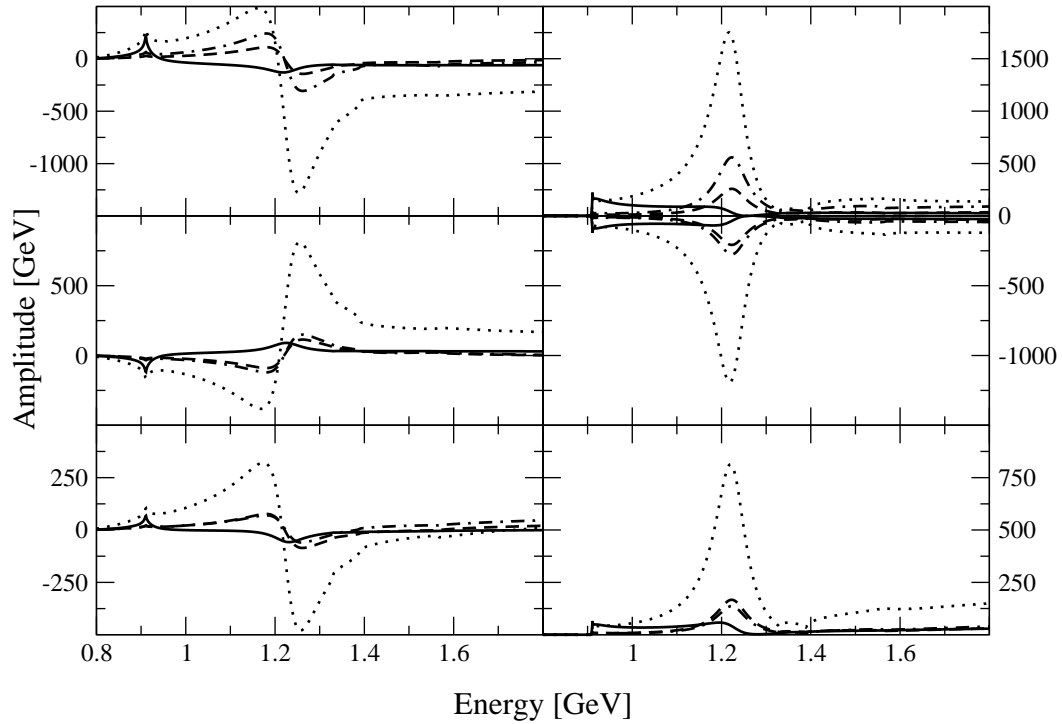


Figure 6.3: This figure shows the amplitudes for $(I^G, S) = (0^-, 0)$ when only the Weinberg-Tomozawa interaction is considered. The left column shows the real part, the second column the imaginary part of the scattering amplitude. The first row corresponds to the s-wave, the second row to the transition amplitude between s- and d-wave and the last row to d-wave. The solid line corresponds to the $\pi\rho$ channel, the dashed line to $\eta\omega$, the dotted line to $\bar{K}K^*$ and the dash-dotted line to $\eta\phi$.

6.1.3 $(I^G, S) = (0^-, 0)$

In this sector there are two clear signals. The one at higher energies has the properties

mass	width	wave	$\pi \rho$	$\eta \omega$	$\bar{K} K^*$	$\eta \phi$	(6.4)
1.225 GeV	85 MeV	s	1.4	2.5	6.4	3.6	
		$s - d$	1.1	2.0	4.8	2.3	
		d	0.94	1.6	3.6	1.5	

The other signal lies on top of the $\pi \rho$ -threshold at 908 MeV and is dominated by the $\pi \rho$ and the $\bar{K} K^*$ channel. The PDG [30] lists the $h_1(1170)$ with a width of 360 MeV and the $h_1(1380)$ with a width of 90 MeV. These two resonances already were overbound in the previous calculations [15], this problem has even worsened.

6.1.4 $(I^G, S) = (1^+, 0)$

In the $(I^G, S) = (1^+, 0)$ sector the PDG lists the $b_1(1235)$ with a width of 142 MeV. In the calculated spectrum a resonance with the following properties are found:

mass	width	wave	$\pi \omega$	$\pi \phi$	$\eta \rho$	$K \bar{K}^*$	(6.5)
1.304 GeV	92 MeV	s	1.0	1.6	2.7	5.0	
		$s - d$	0.81	0.97	2.2	3.4	
		d	0.64	0.72	1.7	2.3	

This is a good place to pause and take a look at the influence of the parameters of the model. The following table lists the results when a single parameter is changed to the value indicated in the first column.

Scenario	mass[GeV]	width[MeV]	wave	$\pi \omega$	$\pi \phi$	$\eta \rho$	$K \bar{K}^*$	(6.6)
only s - wave	1.265	114	s	1.1	1.8	3.0	5.7	
$b_D = 0.92$	1.338	90	s	1.4	1.5	2.4	5.2	
			$s - d$	1.1	0.84	1.9	3.5	
			s	0.83	0.52	1.5	2.4	
$g_D = 0.5$	1.259	147	s	1.7	1.6	3.5	6.4	
			$s - d$	1.3	0.96	3.0	4.6	
			s	1.0	0.61	2.5	3.4	
$g_F = -0.5$	1.259	112	s	1.2	1.8	3.2	5.9	
			$s - d$	0.94	1.1	2.7	4.2	
			s	0.74	0.72	2.3	3.1	
$\Lambda_S = 1.8 \text{ GeV}$	1.265	113	s	1.2	1.8	3.1	5.6	
			$s - d$	0.93	1.1	2.5	3.8	
			s	0.74	0.71	2.0	2.6	

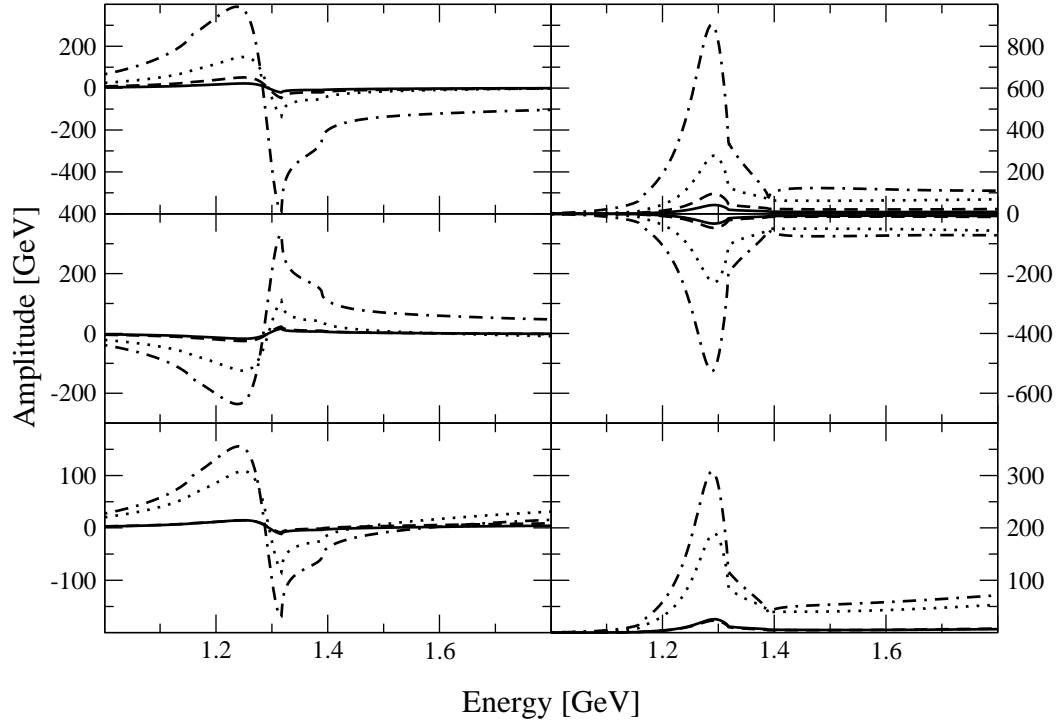


Figure 6.4: This figure shows the amplitudes for $(I^G, S) = (1^+, 0)$ when only the Weinberg-Tomozawa interaction is considered. The left column shows the real part, the second column the imaginary part of the scattering amplitude. The first row corresponds to the s-wave, the second row to to the transition amplitude between s- and d-wave and the last row to d-wave. The solid line corresponds to the $\pi\omega$ channel, the dashed line to $\pi\phi$, the dotted line to $\eta\rho$ and the dash-dotted line to $\bar{K}K^*$.

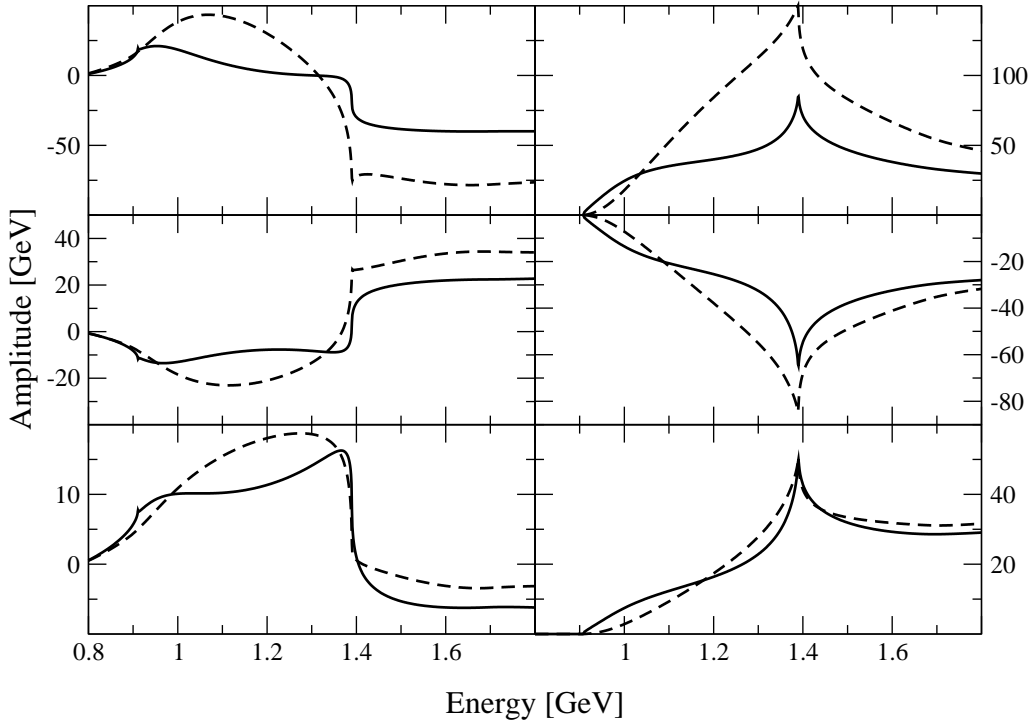


Figure 6.5: This figure shows the amplitudes for $(I^G, S) = (1^-, 0)$ when only the Weinberg-Tomozawa interaction is considered. The left column show the real part, the second column the imaginary part of the scattering amplitude. The first row corresponds to the s-wave, the second row to to the transition amplitude between s- and d-wave and the last row to d-wave. The solid line corresponds to the $\pi \rho$ channel and the dashed line to $\bar{K} K^*$.

Again, omitting the d-wave lowers the mass of the resonance. With about 40 MeV the effect is larger than the 15 MeV found in the channels discussed previously. Even so the mass is lowered, the width is increased.

Setting $b_D = 0.92$ shifts the mass away from its physical value without changing the width. The values 0.5 and -0.5 for g_D and g_F both have an identical effect of the mass, but the width is increased further by the change in g_D , reflecting a stronger coupling to the lightest channel. An increase of the upper bound of the xipansion by 100 MeV has an effect very similar to the change of g_F listed above.

6.1.5 $(I^G, S) = (1^-, 0)$

In the $(I^G, S) = (1^-, 0)$ sector the PDG lists the $a_1(1260)$ with a width of 250-600 MeV. Between the two thresholds at 908 MeV and 1390 MeV a structure can be seen. A quantitative analysis is not possible and will be avoided. A detailed discussion on the nature of the a_1 in the framework of coupled-channels can be found in [31, 32].

In summary the previous results [15] can be reproduced in the new formalism. The approximation to omit the kinematically suppressed d-wave turns out to be justified, as expected from physical reasons.

6.2 Results for the full interaction

In this section the results will be discussed in the case when the full interaction (except the pseudoscalar u -channel) is taken into account.

6.2.1 $(I^G, S) = (1^+, 0)$: the $b_1(1235)$

In this sector there is a clear signal of the $b_1(1235)$. The PDG lists it with a mass of 1229.5 ± 3.2 MeV and a width of 142 ± 9 MeV [30]. In the previous work [19] the values $g_D = 0.7$ and $g_F = -2.8$ were necessary to reproduce the experimental value for this resonance that came out 100 MeV too heavy and was also too broad.

In a first step the results will be discussed when only s-wave and the zeroth order in the xipansion is considered. This means that all contributions that are not caused by cuts inside the xipansion area will be set to their value at the xipansion point $\frac{1}{2}(m + M + \bar{m} + \bar{M})$, i.e. constant. When only the Weinberg-Tomozawa interaction is considered, the molecule comes out at a too high energy, just like as in [19]. The structure overlaps with the $K \bar{K}^*$ threshold. Adding the t - and u -channel has very little effect on the amplitude. Once the s -channel is added, the resonance is gone. To undo this repulsive effect and bring the resonance down to its physical value, large values for the counter-terms are necessary: $g_D = 4.15$ and $g_F = -5.75$. This will lead to the amplitudes shown in fig. 6.6.

Since $K \bar{K}^*$ is the dominant channel it will be discussed in a little more detail. Without the u -channel there is no cut inside the xipansion region and therefor the potential is constant. The size of the contributions is the following:

$$\begin{array}{cc|cc|ccc} WT & b_D & g_D & g_F & S - ch & T - ch & U - ch \\ 70.4 & 18.0 & 58.6 & -19.5 & -143 & 0.0007 & -3.0 \end{array}, \quad (6.7)$$

where the units are GeV and for example g_D indicates the value 58.6 GeV for the counter term with $g_D = 4.15$. The extremely small value for the t -channel is caused by a root in the exact potential near the xipansion point. The table above shows that the s -channel reverses the effect of the Weinberg-Tomozawa interaction which is why the counter terms have to take such large values ¹.

¹For the s -channel there are two vector-vector-pseudoscalar vertices present resulting in a total of four diagrams. In the $K \bar{K}^*$ channel they all add up coherently, explaining the large contribution.

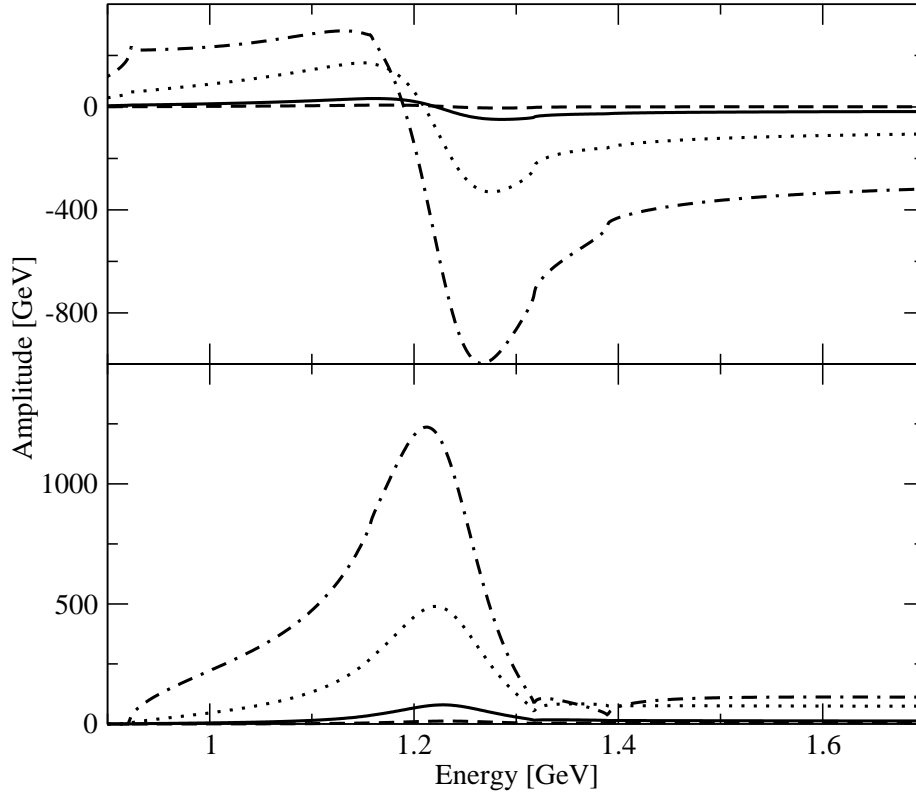


Figure 6.6: This figure shows the amplitudes for $(I^G, S) = (1^+, 0)$ when the full tree level scattering amplitude in equ. (3.10) (excluding the pseudoscalar u -channel) is considered to zeroth order in the expansion. The upper graph corresponds to the real part of the amplitude while the lower one shows the imaginary part. The solid line corresponds to the $\pi\omega$ channel, the dashed line to $\pi\phi$, the dotted line to $\eta\rho$ and the dash-dotted line to $\bar{K}K^*$.

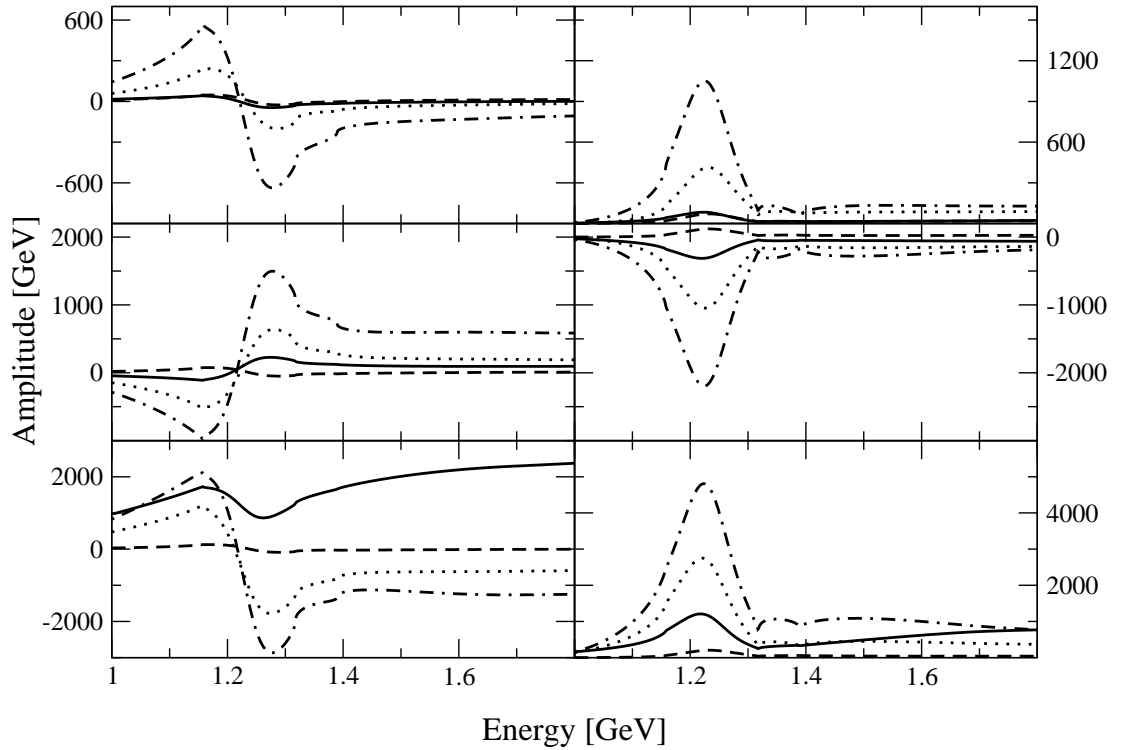


Figure 6.7: This figure shows the amplitudes for $(I^G, S) = (1^+, 0)$ when the full tree level scattering amplitude in equ. (3.10) (excluding the pseudoscalar u -channel) is considered to first order in the expansion. The upper graph corresponds to the real part of the amplitude while the lower one shows the imaginary part. The solid line corresponds to the $\pi\omega$ channel, the dashed line to $\pi\phi$, the dotted line to $\eta\rho$ and the dash-dotted line to $\bar{K}K^*$.

The situation changes when the first order of the expansion is included. The result for Weinberg-Tomozawa was already presented, with a mass of 1.304 GeV it was almost 70 MeV above the physical value. To reproduce the physical mass and width, the parameters $g_D = 0.7$ and $g_F = 2.8$ were necessary in [19]. These values are a good starting point for the fit in the present scenario. Here the b_1 can be reproduced with the values $g_D = 0.8$ and $g_F = -3.56$, the result is shown in fig. 6.7.

The contributions to the most important process $K\bar{K}^* \rightarrow K\bar{K}^*$ are illustrated in fig. 6.8.

In summary the results are

Scenario	g_D	g_F	mass[GeV]	width[MeV]	$\pi\omega$	$\pi\phi$	$\rho\eta$	$K\bar{K}^*$
xiorder 0	4.15	-5.75	1.230	135	1.8	0.73	4.4	6.9
xiorder 1					1.9	1.8	4.3	6.9
s + d wave	0.8	-3.56	1.231	138	3.2	2.1	6.1	8.7
					6.0	2.4	8.6	11.2
[19]	0.7	-2.8	1.230	142	2.1	1.0	2.3	4.2

(6.8)

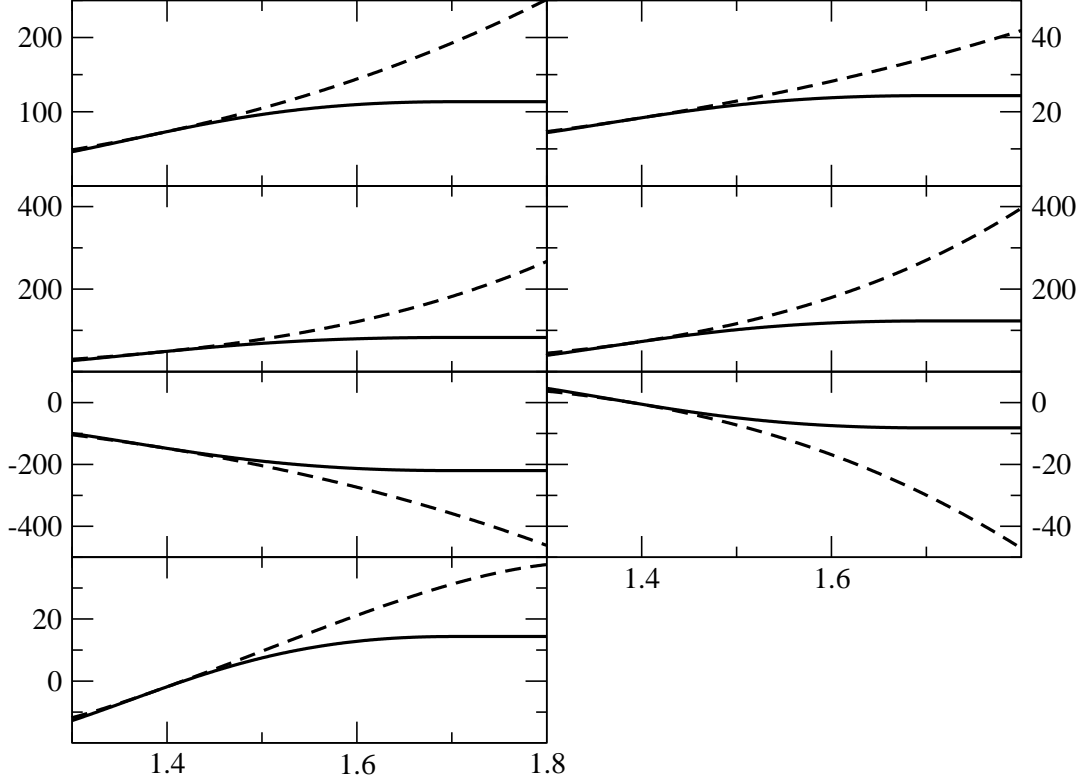


Figure 6.8: This figure shows the amplitudes for the process $K \bar{K}^* \rightarrow K \bar{K}^*$ with $(I^G, S) = (1^+, 0)$ using the counter terms specified in 6.8. The first row shows the Weinberg-Tomozawa interaction (left) and the term which is multiplied by b_D , the second line shows the interactions multiplied by g_D and g_F (with the fitted value of equ. 6.8), the third line shows the s - and t -channel contributions to the potential and the last line illustrates the u -channel. Solid lines correspond to the xipanded potential actually used while the dashed lines indicate the exact potential without xipansion. The xipansion point is the $K \bar{K}^*$ threshold at 1.39 GeV, the potential is not needed below that point.

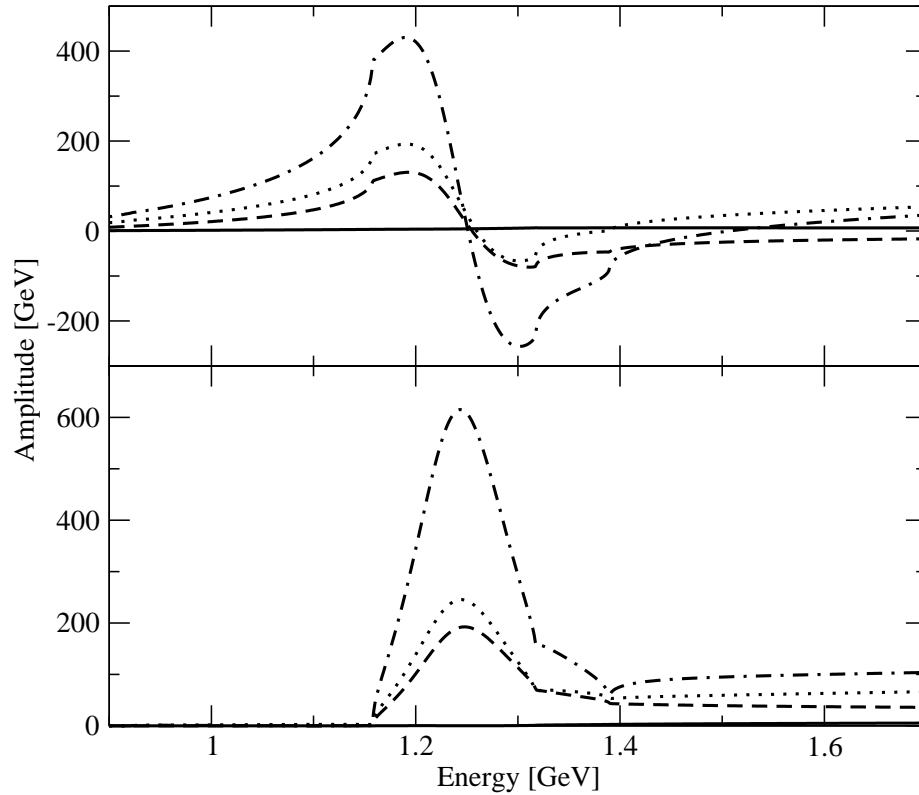


Figure 6.9: This figure shows the amplitudes for $(I^G, S) = (1^+, 0)$ when the full tree level scattering amplitude in equ. (3.10) (excluding the pseudoscalar u -channel) is considered to first order in the xipansion. The upper graph corresponds to the real part of the amplitude while the lower one shows the imaginary part. The solid line corresponds to the $\pi\omega$ channel, the dashed line to $\pi\phi$, the dotted line to $\eta\rho$ and the dash-dotted line to $\bar{K}K^*$.

The size of the counter terms is only reasonable (and in line with [19]) when the first order of the xipansion is considered. The open $\pi\phi$ channel plays a more important role when all helicities and the first order of the xipansion are considered while the dominant decay channel $\pi\omega$ remains almost unchanged compared to the previous work [19].

6.2.2 $(I, S) = (\frac{1}{2}, 1)$: the $K_1(1270)$

In this sector the previous work [15] found two resonances, the $K_1(1270)$ which has a width of 90 MeV and the $K_1(1400)$ with a width of 174 MeV. In the more detailed analysis [19] the coupling constants of the counter terms had to be set to $g_D = 0.2$ and $g_F = -0.1$. Fig. 6.10 shows the result when these two couplings are set to zero. A clear signal can be seen close to the nominal ρK threshold at 1.266 GeV and the nominal ωK threshold at 1.278 GeV. The width of the ρ meson will have a considerable effect on the width of

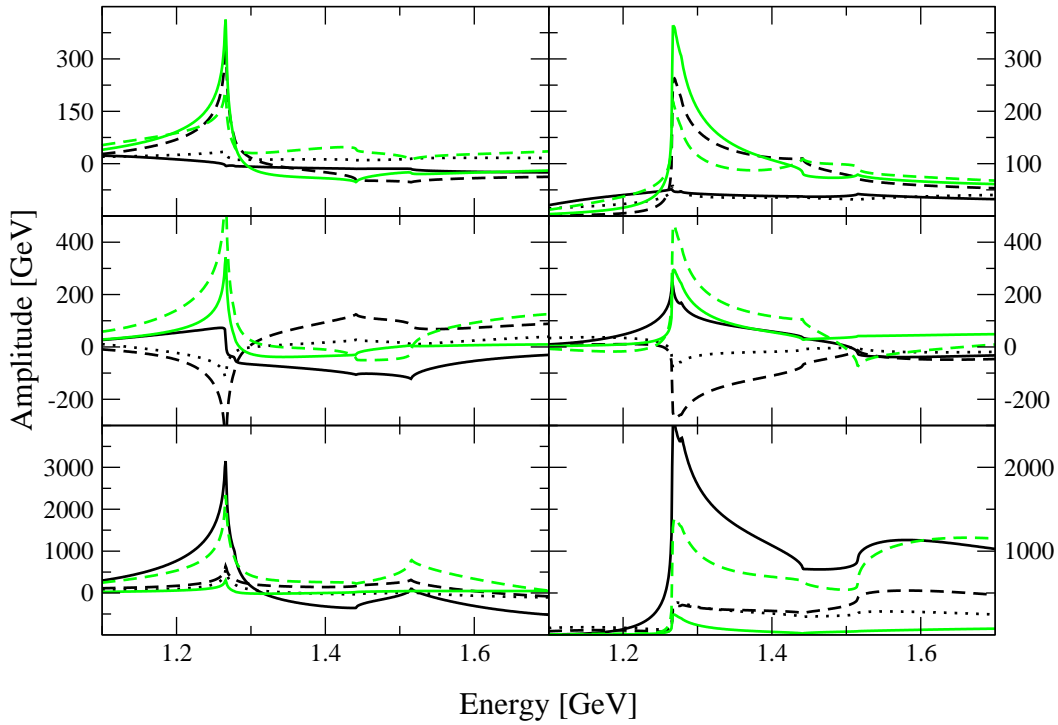


Figure 6.10: This figure shows the amplitudes for $(I^G, S) = (\frac{1}{2}, 1)$ when all interactions except the pseudoscalar exchanges are considered. The couplings of the counter-terms, g_D and g_F are put to zero. The left column show the real part, the second column the imaginary part of the scattering amplitude. The first row corresponds to the s-wave, the second row to to the transition amplitude between s- and d-wave and the last row to d-wave. The solid black line corresponds to the πK channel, the dashed black line to ρK , the dotted black line to ωK , the solid green line to ηK^* and the dashed green line to ϕK .

the resonance, therefore we will not try to fit the resonance calculated with sharp masses to the data more accurately. Nevertheless it is encouraging that the result with all interactions and no counter terms closely resembles the result of [15] which agreed well with experimental data once the width of the vector mesons was taken into account (see fig. 2 in [15]).

Chapter 7

Summary and Outlook

In this work we studied the scattering of the lightest octet of pseudoscalar mesons, the pion, the K-meson and the eta, off the nonet of vector mesons which includes the ρ meson. A formalism based on a non-linear integral equation is used to compute scattering amplitudes. Solutions of the non-linear integral equations comply with constraints set by causality and unitarity. The main input into this equation are pretreated tree-level scattering amplitudes that were derived in the following steps: an interaction Lagrangian based on chiral and large N_c arguments was utilized to calculate the tree level amplitudes. It included the Weinberg-Tomozawa interaction, three counter terms and the exchange of vector mesons in the s -, t - and u -channel. The exchange of pseudoscalar mesons was not considered in the final calculation because of technical challenges. It was illustrated how these issues can be mastered in principle but the actual calculation was beyond the scope of this work.

The tree level amplitudes were then partial-wave projected and extrapolated to higher energies based on the knowledge of their analytic structure. These modified potentials define the input of the non-linear integral equations.

In a first step, the spectrum was calculated for the Weinberg-Tomozawa interaction only and compared to the previous results. The influence of the counter terms and the order of the analytical extrapolation of the scattering amplitude were addressed. Then the spectrum for the full interaction was discussed in sectors of particular interest. Counter-terms were adjusted to reproduce the mass and width of the $b_1(1235)$ exactly. In addition, the $K_1(1270)$ was investigated in more detail. Its mass is recovered in the absence of any counter term. This is in conflict with the significant size of the counter terms obtained from the study of the $b_1(1235)$. We take this asymmetry as a consequence of the absence of the pseudoscalar u -channel.

The most obvious extension of this work is the inclusion of these pseudoscalar exchange processes. One possible way to achieve this has already been discussed, but improvements are desirable, especially to keep the necessary CPU-time in reasonable limits. Including these processes we expect that a reliable computation of the D/S ratios in the decays of the axial resonances

is feasible.

Another interesting possibility is the inclusion of vector-vector and pseudoscalar-pseudoscalar channels. From a formal point of view these channels can be treated analogously. The partial wave projection will become more tedious. With all these channels included it is interesting to calculate resonances with other spin and parity than just 1^+ with relatively little additional effort.

In summary the formalism employed in this thesis reproduces the measured spectrum and previous results within reasonable limits. It also allows to use a more realistic interaction and to include more channels in a consistent way so that in future works more physical systems become accessible as well as a wider variety of observables.

Appendix A

The invariant amplitude

In this appendix we give explicit expressions for the G 's which result from the partial-wave projection of equ. (3.10). Only non-vanishing G 's are shown with one exception: if G_3 does not vanish, then G_4 is the hermitian conjugate (incoming and outgoing masses interchanged) unless displayed explicitly.

A.1 The 4-point vertices

The invariant amplitudes for the contact interactions are given by

$$\begin{aligned}
 G_1 = & \frac{C_{WT}}{4 \bar{M} M f^2} \left((\bar{m}^2 - s + \frac{1}{2}(M^2 + \bar{M}^2 - t)) M^2 \right. \\
 & \left. + (m^2 - s + \frac{1}{2}(\bar{M}^2 + M^2 - t)) \bar{M}^2 \right) \\
 & - \frac{g_D C_D + g_F C_F}{32 f^2 \bar{M} M} (m^2 + \bar{m}^2 - t) (M^2 + \bar{M}^2 - t) \\
 & - \frac{b_D C_\chi}{16 f^2 \bar{M} M} (M^2 + \bar{M}^2 - t) , \tag{A.1}
 \end{aligned}$$

$$G_3 = \frac{C_{WT} M}{2 f^2 \bar{M}} , \tag{A.2}$$

$$\begin{aligned}
 G_5 = & - \frac{C_{WT} (M^2 + \bar{M}^2)}{4 f^2 \bar{M} M} \\
 & + \frac{g_D C_D + g_F C_F}{16 f^2 \bar{M} M} (m^2 + \bar{m}^2 - t) \\
 & + \frac{b_D C_\chi}{8 f^2 \bar{M} M} . \tag{A.3}
 \end{aligned}$$

A.2 The Pseudoscalar s-channel Exchange

For the s-channel exchange of a pseudoscalar meson the invariant amplitudes are given by

$$G_2 = - \left(\frac{m_V h_P}{2 f^2} \right)^2 \frac{C_{s-ch}^{(x)} \bar{M} M}{s - m_x^2}. \quad (\text{A.4})$$

A.3 The Pseudoscalar u-channel Exchange

For the u -channel exchange of a pseudoscalar meson the invariant amplitudes are given by

$$G_2 = - \left(\frac{m_V h_P}{2 f^2} \right)^2 \frac{C_{u-ch}^{(x)} \bar{M} M}{u - m_x^2}, \quad (\text{A.5})$$

$$G_3 = \left(\frac{m_V h_P}{2 f^2} \right)^2 \frac{C_{u-ch}^{(x)} \bar{M} M}{u - m_x^2}, \quad (\text{A.6})$$

$$G_5 = - \left(\frac{m_V h_P}{2 f^2} \right)^2 \frac{C_{u-ch}^{(x)} \bar{M} M}{u - m_x^2}. \quad (\text{A.7})$$

A.4 The s-channel Vector Exchange

The exchange of a vector meson in the s-channel has several contributions. The interaction labeled (11) results in the following invariant amplitudes:

$$\begin{aligned} G_1 = & \frac{C_{s-ch}^{(11,x)} h_A^2}{4 f^2 \bar{M} M m_x^2} \left(- m_x^2 (p \cdot \bar{p}) (M^2 + \bar{M}^2 + m_x^2 + s) \right. \\ & \left. + (m_x^2 (w \cdot \bar{p}) (w \cdot p) - \bar{M}^2 M^2 ((w \cdot \bar{p}) + (w \cdot p) - s)) \right) + \\ & \frac{1}{(m_x^2 - s)} \left\{ (\bar{M}^2 + m_x^2) (M^2 + m_x^2) (m_x^2 (p \cdot \bar{p}) - (w \cdot \bar{p}) (w \cdot p)) \right\} \end{aligned} \quad (\text{A.8})$$

$$\begin{aligned} G_2 = & - \frac{C_{s-ch}^{(11,x)} h_A^2}{4 f^2 \bar{M} M m_x^2} \left(((\bar{M}^2 M^2) - m_x^2 (p \cdot \bar{p})) \right. \\ & \left. + \frac{1}{(m_x^2 - s)} \left\{ (\bar{M}^2 + m_x^2) (M^2 + m_x^2) (p \cdot \bar{p}) \right\} \right), \end{aligned} \quad (\text{A.9})$$

$$G_3 = \frac{C_{s-ch}^{(11,x)} h_A^2}{4 f^2 \bar{M} M m_x^2} \left((\bar{M}^2 M^2 - m_x^2 (w \cdot p)) \right)$$

$$+\frac{1}{(m_x^2 - s)} \left\{ (\bar{M}^2 + m_x^2) (M^2 + m_x^2) (w \cdot p) \right\}, \quad (\text{A.10})$$

$$G_5 = \frac{C_{s-ch}^{(11,x)} h_A^2}{4 f^2 \bar{M} M} \left((\bar{M}^2 + M^2 + m_x^2 + s) - \frac{1}{m_x^2 - s} \left\{ (\bar{M}^2 + m_x^2) (M^2 + m_x^2) \right\} \right). \quad (\text{A.11})$$

The interaction labeled (12) results in the following invariant amplitudes:

$$G_1 = \frac{C_{s-ch}^{(12,x)} b_A h_A}{f^2 \bar{M} M m_x^2} \left((m_x^2 (p \cdot \bar{p}) + \bar{M}^2 (w \cdot p)) - \frac{1}{m_x^2 - s} \left\{ (\bar{M}^2 + m_x^2) (m_x^2 (p \cdot \bar{p}) - (w \cdot \bar{p}) (w \cdot p)) \right\} \right), \quad (\text{A.12})$$

$$G_2 = \frac{C_{s-ch}^{(12,x)} b_A h_A}{f^2 \bar{M} M m_x^2} \frac{1}{m_x^2 - s} \left\{ (\bar{M}^2 + m_x^2) (p \cdot \bar{p}) \right\}, \quad (\text{A.13})$$

$$G_3 = -\frac{C_{s-ch}^{(12,x)} b_A h_A}{f^2 \bar{M} M m_x^2} \frac{1}{m_x^2 - s} \left\{ (\bar{M}^2 + m_x^2) (w \cdot p) \right\}, \quad (\text{A.14})$$

$$G_4 = -\frac{C_{s-ch}^{(12,x)} b_A h_A}{f^2 \bar{M} M m_x^2} \left(\bar{M}^2 + \frac{1}{m_x^2 - s} \left\{ (\bar{M}^2 + m_x^2) (w \cdot \bar{p}) \right\} \right), \quad (\text{A.15})$$

$$G_5 = \frac{C_{s-ch}^{(12,x)} b_A h_A}{f^2 \bar{M} M m_x^2} \left(-m_x^2 + \frac{1}{m_x^2 - s} \left\{ (\bar{M}^2 + m_x^2) m_x^2 \right\} \right). \quad (\text{A.16})$$

$$(\text{A.17})$$

The invariant amplitudes for the (21) interaction can be derived from those for the (12) interaction by interchanging incoming and outgoing particles, $C^{(12,x)}$ and $C^{(21,x)}$ and finally G_3 and G_4 .

The interaction labeled (22) results in the following invariant amplitudes:

$$G_1 = \frac{4 b_A^2 C_{s-ch}^{(22,x)} m_x^2 (p \cdot \bar{p}) - (w \cdot \bar{p}) (w \cdot p)}{f^2 \bar{M} M m_x^2 (m_x^2 - s)}, \quad (\text{A.18})$$

$$G_2 = -\frac{4 b_A^2 C_{s-ch}^{(22,x)} (p \cdot \bar{p})}{f^2 \bar{M} M m_x^2 (m_x^2 - s)}, \quad (\text{A.19})$$

$$G_3 = \frac{4 b_A^2 C_{s-ch}^{(22,x)} (w \cdot p)}{f^2 \bar{M} M m_x^2 (m_x^2 - s)}, \quad (\text{A.20})$$

$$G_5 = -\frac{4 b_A^2 C_{s-ch}^{(22,x)} m_x^2}{f^2 \bar{M} M m_x^2 (m_x^2 - s)}. \quad (\text{A.21})$$

$$(\text{A.22})$$

A.5 The t-channel Vector Exchange

For the t-channel exchange of a vector meson the invariant amplitudes are given by the sum of two contributions, the first one being

$$G_1 = \frac{3 C_{t-ch}^{(x)} h_P h_V m_V^2}{8 f^2 \bar{M} M} \left((m_x^2 + s - u) + \frac{1}{t - m_x^2} \{ m_x^4 + m_x^2 (s - t - u) + (m^2 - \bar{m}^2) (M^2 - \bar{M}^2) \} \right), \quad (\text{A.23})$$

$$G_3 = \frac{3 C_{t-ch}^{(x)} h_P h_V m_V^2}{2 f^2 \bar{M} M} \frac{-M^2}{t - m_x^2}, \quad (\text{A.24})$$

$$G_5 = \frac{3 C_{t-ch}^{(x)} h_P h_V m_V^2}{4 f^2 \bar{M} M} \left(1 + \frac{1}{t - m_x^2} \{ 2s + m_x^2 - m^2 - \bar{m}^2 \} \right), \quad (\text{A.25})$$

and the second one

$$G_1 = \frac{C_{t-ch}^{(x)} h_P \tilde{h}_V}{8 f^2 \bar{M} M} (M^2 + \bar{M}^2) \left((m_x^2 + s - u) + \frac{1}{t - m_x^2} \{ m_x^4 + m_x^2 (s - t - u) + (m^2 - \bar{m}^2) (M^2 - \bar{M}^2) \} \right), \quad (\text{A.26})$$

$$G_3 = -\frac{C_{t-ch}^{(x)} h_P \tilde{h}_V}{2 f^2 \bar{M} M} \left(M^2 + \frac{1}{t - m_x^2} \{ M^2 \bar{M}^2 + M^2 m_x^2 \} \right), \quad (\text{A.27})$$

$$G_5 = \frac{C_{t-ch}^{(x)} h_P \tilde{h}_V}{4 f^2 \bar{M} M} \left((M^2 + \bar{M}^2) + \frac{1}{t - m_x^2} \{ m_x^2 (M^2 + \bar{M}^2) - (m^2 - \bar{m}^2) (M^2 - \bar{M}^2) + 2 \bar{M}^2 M^2 \} \right) \quad (\text{A.28})$$

A.6 The u-channel Vector Exchange

The exchange of a vector meson in the u-channel has several contributions. The interaction labeled (11) results in the following invariant amplitudes:

$$G_1 = \frac{C_{u-ch}^{(11,x)} h_A^2}{16 f^2 \bar{M} M m_x^2} \left(-m_x^6 + m_x^4 (\bar{m}^2 + m^2 - 2s - u) + m_x^2 ((M^2 + \bar{M}^2) (M^2 + \bar{M}^2 - 2s) + u (m^2 + \bar{m}^2 - 2s)) \right)$$

$$\begin{aligned}
& +m^2\bar{M}^2 + m^2\bar{m}^2 + M^2\bar{m}^2) \\
& +\bar{M}^2M^2(u + m^2 + \bar{m}^2 - \bar{M}^2 - M^2) \\
& + \frac{1}{u - m_x^2} \left\{ (\bar{M}^2 + m_x^2)(M^2 + m_x^2)((M^2 - \bar{m}^2)(\bar{M}^2 - m^2) \right. \\
& \left. + m_x^2(m^2 + M^2 + \bar{m}^2 + \bar{M}^2 - 2s - m_x^2)) \right\}, \tag{A.29}
\end{aligned}$$

$$\begin{aligned}
G_2 &= \frac{C_{u-ch}^{(11,x)} h_A^2}{8 f^2 \bar{M} M m_x^2} \left(m_x^4 + m_x^2 (2M^2 + 2\bar{M}^2 - t) - M^2 \bar{M}^2 \right. \\
& \left. + \frac{1}{u - m_x^2} \left\{ (\bar{M}^2 + m_x^2)(M^2 + m_x^2)(s + m_x^2 - m^2 - \bar{m}^2) \right\} \right), \tag{A.30}
\end{aligned}$$

$$\begin{aligned}
G_3 &= \frac{C_{u-ch}^{(11,x)} h_A^2}{8 f^2 \bar{M} M m_x^2} \left(m_x^2 (m^2 + M^2 - s) \right. \\
& \left. + \frac{1}{u - m_x^2} \left\{ (m_x^4 + M^2 m_x^2 + \bar{M}^2 m_x^2 + M^2 \bar{M}^2) (m^2 + M^2 - s) \right\} \right) \tag{A.31}
\end{aligned}$$

$$\begin{aligned}
G_5 &= \frac{C_{u-ch}^{(11,x)} h_A^2}{8 f^2 \bar{M} M m_x^2} \left((M^2 \bar{M}^2 + m_x^2 (m_x^2 + s + u)) \right. \\
& - \frac{1}{u - m_x^2} \left\{ (m_x^4 + M^2 m_x^2 + \bar{M}^2 m_x^2 + M^2 \bar{M}^2) \right. \\
& \left. \left. \cdot (M^2 + \bar{M}^2 - m_x^2 - s) \right\} \right). \tag{A.32}
\end{aligned}$$

The interaction labeled (12) results in the following invariant amplitudes:

$$\begin{aligned}
G_1 &= -\frac{C_{u-ch}^{(12,x)} h_A b_A}{4 f^2 \bar{M} M m_x^2} \left(-m_x^4 + m_x^2 (m^2 + M^2 + \bar{m}^2 - 2s - u) \right. \\
& \left. + \bar{M}^2 (\bar{M}^2 - m^2 - M^2 - u + \bar{m}^2) \right. \\
& \left. + \frac{1}{u - m_x^2} \left\{ -m_x^6 + m_x^4 (m^2 + M^2 + \bar{m}^2 - 2s) \right. \right. \\
& \left. \left. + m_x^2 (\bar{M}^4 - m^2 M^2 + m^2 \bar{m}^2 + m^2 \bar{M}^2 + 2M^2 \bar{M}^2 - 2\bar{M}^2 s) \right. \right. \\
& \left. \left. + \bar{M}^2 (M^2 - \bar{m}^2) (\bar{M}^2 - m^2) \right\} \right), \tag{A.33}
\end{aligned}$$

$$\begin{aligned}
G_2 &= -\frac{C_{u-ch}^{(12,x)} h_A b_A}{2 f^2 \bar{M} M m_x^2} \left((\bar{M}^2 + m_x^2) \right. \\
& \left. + \frac{1}{u - m_x^2} \left\{ (\bar{M}^2 + m_x^2) (-m^2 - \bar{m}^2 + m_x^2 + s) \right\} \right), \tag{A.34}
\end{aligned}$$

$$G_3 = -\frac{C_{u-ch}^{(12,x)} h_A b_A}{2 f^2 \bar{M} M m_x^2} \frac{1}{u - m_x^2} \left\{ (\bar{M}^2 + m_x^2) (m^2 + M^2 - s) \right\}, \tag{A.35}$$

$$\begin{aligned}
G_4 &= \frac{C_{u-ch}^{(12,x)} h_A b_A}{2 f^2 \bar{M} M m_x^2} \left(2\bar{M}^2 \right. \\
& \left. + \frac{1}{u - m_x^2} \left\{ (\bar{M}^2 + m_x^2) (s - \bar{M}^2 - \bar{m}^2) \right\} \right), \tag{A.36}
\end{aligned}$$

$$\begin{aligned}
G_5 &= \frac{C_{u-ch}^{(12,x)} h_A b_A}{2 f^2 \bar{M} M m_x^2} \left(- (\bar{M}^2 + m_x^2) \right. \\
&\quad \left. + \frac{1}{u - m_x^2} \left\{ (\bar{M}^2 + m_x^2) (M^2 + \bar{M}^2 - m_x^2 - s) \right\} \right). \tag{A.37}
\end{aligned}$$

The invariant amplitudes for the (21) interaction can be derived from those for the (12) interaction by interchanging incoming and outgoing particles, $C^{(12,x)}$ and $C^{(21,x)}$ and finally G_3 and G_4 .

The interaction labeled (22) results in the following invariant amplitudes:

$$\begin{aligned}
G_1 &= \frac{C_{u-ch}^{(22,x)} b_A^2}{f^2 \bar{M} M m_x^2} \left(- m^2 + M^2 - \bar{m}^2 + \bar{M}^2 - m_x^2 + u \right. \\
&\quad \left. + \frac{1}{u - m_x^2} \left\{ - m_x^4 + m_x^2 (m^2 + M^2 + \bar{m}^2 + \bar{M}^2 - 2s) \right. \right. \\
&\quad \left. \left. + (M^2 - \bar{m}^2)(\bar{M}^2 - m^2) \right\} \right), \tag{A.38}
\end{aligned}$$

$$G_2 = \frac{2 C_{u-ch}^{(22,x)} b_A^2}{f^2 \bar{M} M m_x^2} \left(1 + \frac{1}{u - m_x^2} \left\{ - m^2 - \bar{m}^2 + m_x^2 + s \right\} \right), \tag{A.39}$$

$$G_3 = \frac{2 C_{u-ch}^{(22,x)} b_A^2}{f^2 \bar{M} M m_x^2} \frac{1}{u - m_x^2} \left\{ m^2 + M^2 - s \right\}, \tag{A.40}$$

$$G_5 = - \frac{2 C_{u-ch}^{(22,x)} b_A^2}{f^2 \bar{M} M m_x^2} \left(1 + \frac{1}{u - m_x^2} \left\{ M^2 + \bar{M}^2 - m_x^2 - s \right\} \right). \tag{A.41}$$

Bibliography

- [1] S. Godfrey, N. Isgur, Phys. Rev. **D 32** (1985) 189-231.
- [2] S. Capstick, N. Isgur, Phys. Rev. **D 34** (1986) 2809-2835.
- [3] E.S. Swanson, Phys. Rept. **429** (2006) 243-305.
- [4] R.H. Dalitz and S.F. Tuan., Phys. Rev. Lett. **2** (1959).
- [5] E.E. Kolomeitsev, M.F.M. Lutz, Nucl. Phys. **A 700** (2002) 193-308.
- [6] U.-G. Meissner et al., Nucl. Phys. **A 755** (2005) 669-672.
- [7] E.E. Kolomeitsev, M.F.M. Lutz, Nucl. Phys. **A 730** (2004) 110-120.
- [8] J. Hofmann, M.F.M. Lutz, Nucl. Phys. **A 763** (2005) 90-139.
- [9] E.E. Kolomeitsev, M.F.M. Lutz, Phys. Lett. **B 585** (2004) 243-252.
- [10] J. Hofmann, M.F.M. Lutz, Nucl. Phys. **A 776** (2006) 17-51.
- [11] L. Roca et al., Phys. Rev. **C 73** (2006) 045208.
- [12] E.E. Kolomeitsev, M.F.M. Lutz, Phys. Lett. **B 582** (2004) 39-48.
- [13] J. Hofmann, M.F.M. Lutz, Nucl. Phys. **A 733** (2003) 142-152.
- [14] M.F.M. Lutz, M. Soyeur, Nucl. Phys. **A 813** (2008) 14-95.
- [15] E.E. Kolomeitsev, M.F.M. Lutz, Nucl.Phys. **A 730** (2004) 392-416.
- [16] L. Roca, E. Oset, J. Singh, Phys. Rev. **D 72** (2005) 014002.
- [17] E. Oset et al., Phys. Rev. **D 76** (2007) 074016
- [18] M.F.M. Lutz, E.E. Kolomeitsev, in preparation.
- [19] M.F.M. Lutz, S. Leupold, Nucl. Phys. **A 813** (2008) 96-170.
- [20] G. 't Hooft, Nucl. Phys. **B 72** (1964) 461.
- [21] A. V. Manohar, hep-ph/9802419v1.

- [22] S. Weinberg, *The Quantum Theory of Fields : Vol. 2*, Cambridge UP, 2005.
- [23] S. Scherer, *Adv. Nucl. Phys.* **27** (2003) 277.
- [24] A. Krause, *Helv. Phys. Acta* **63** (1990) 3.
- [25] A.M. Badalyan et al., *Phys. Rept.* **82** (1982) 31-177.
- [26] N.I. Muskhelishvili, *Singular integral equations*, Groningen 1953.
- [27] R. Omnes, *Nuov. Cim.* **2** (1958) 316.
- [28] P.W. Johnson, R.L. Warnock, *J. Math. Phys.* **22** (1981) 385.
- [29] M.F.M. Lutz, Gy. Wolf, B. Friman, *Nucl. Phys.* **A 706** (2002) 431-496.
- [30] C. Amsler et al. (Particle Data Group), *Phys. Lett.* **B 667**, 1 (2008).
- [31] M. Wagner, S. Leupold, *Phys. Lett.* **B 670** (2008) 22-26.
- [32] M. Wagner, S. Leupold, *Phys. Rev.* **D 78** (2008) 053001.

Acknowledgements

First of all I would like to thank my adviser Priv. Doz. Dr. Matthias Lutz for the interesting topic and permanent willingness for discussions. Thanks also to Prof. Dr. Wambach for the hospitality at the GSI theory group and for putting me in the position to write this thesis. I also have to mention Prof. Dr. Evgueni Kolomeitsev and Dr. Isaac Vidana for many interesting discussions and important numerical checks. Special thanks to those who kept my computer running, especially Alexander Semke and Dr. Thomas Neff who always provided the necessary support for the calculations. Also I would like to thank my roommates and fellow student for the pleasant atmosphere, especially Alexander Semke, Ashot Gasparyan, Markus Leykauf and Ilka Petermann, my roommates Yonggoo Heo and Igor Danilkin, as well as Dr. Kai Hebel and Dr. Felix Riek.

Erklärung

Hiermit erkläre ich eidesstattlich, dass ich die vorliegende Dissertation selbstständig verfasst, keine anderen als die angegebenen Hilfsmittel verwendet und noch keinen Promotionsversuch unternommen habe.

Darmstadt, den 25 Januar 2010,

Julian Hofmann

Unterschiede zur eingereichten Version

- Kleinere Tippfehler behoben
- Erste Gleichung in Kapitel 4.2 entfernt
- Kapitel 5.2 und 5.3 verschmolzen und gekürzt
- Ein Absatz auf der zweiten Seite von Kapitel 4 entfernt

Lebenslauf

Julian Hofmann
Ledig, keine Kinder

- Geboren am 12. Juni 1980 in Frankfurt
- 1986-1990 Grundschule in Mörfelden-Walldorf
- 1990-1999 Prälat-Diehl-Schule in Groß-Gerau (Sprachen: Englisch, Latein; Abiturnote 1.3)
- 1999-2000 Zivildienst bei der Stadt Mörfelden-Walldorf im Bereich Umweltschutz
- 2000-2002 Grundstudium der Physik an der TU Darmstadt (Gesamturteil "Sehr Gut")
- 2002-2004 Hauptstudium an der TU-Darmstadt
- 2004-2005 Diplomarbeit an der GSI zum Thema "Gekoppelte Kanaldynamik für Resonanzen mit Charm-Quarks" (Note 1.0 mit Auszeichnung)
- seit 2005 Promotion an der GSI